Escherichia coli biofilm formation, motion and protein patterns on hyaluronic acid and polydimethylsiloxane depend on surface stiffness

Annabelle Vigué, Dominique Vautier, Amad Kaytoue, Bernard Senger, Youri Arntz, Vincent Ball, Amine Ben Mlouka, Varvara Gribova, Samar Hajjar-Garreau, Julie Hardouin, et al.

Escherichia coli biofilm formation, motion and protein patterns on hyaluronic acid and polydimethylsiloxane depend on surface stiffness

Annabelle Vigué [1,2], Dominique Vautier [1,2], Amad Kaytoue [1,2], Bernard Senger [1,2], Youri Arntz [1,2], Vincent Ball [1,2], Amine Ben Mlouka [4], Varvara Gribova [1,2], Samar Hajjar-Garreau [5], Julie Hardouin [3,4], Thierry Jouenne [3,4], Philippe Lavalle [1,2] and Lydie Ploux [1,2,6,*]

[1] INSERM UMR-S 1121 Biomaterial Bioengineering, Centre de Recherche en Biomédecine de Strasbourg, Strasbourg, France
[2] University of Strasbourg, Faculty of Dentistry, Strasbourg, France
[3] Normandie University, UNIROUEN, INSA Rouen, CNRS, Polymers, Biopolymers, Surfaces Laboratory, Rouen, France
[4] PISSARO Proteomic Facility, IRIB, Mont-Saint-Aignan, France
[5] CNRS, Haute Alsace University, Mulhouse Materials Science Institute, Mulhouse, France
[6] CNRS, Strasbourg, France
* Correspondence: ploux@unistra.fr

Abstract: Surface stiffness of the microenvironment is a mechanical signal regulating biofilm growth without the risks associated with the use of bioactive agents. However, mechanisms determining the expansion or prevention of biofilm growth on soft and stiff substrates are largely unknown. To answer this question, we used PDMS (polydimethylsiloxane, 9-574kPa) and HA (hyaluronic acid gels, 44Pa-2kPa) differing in hydration. We showed that softest HA inhibits Escherichia coli biofilm growth while stiffest PDMS activates it. The bacterial mechanical environment significantly regulates MscS mechanosensitive channel, in higher abundance on the least colonized HA-44Pa, and Type-1 pili (Fim A) in higher abundance on the most colonized PDMS-9kPa. Type 1 pili regulated free motion (capacity of bacteria to move far from it initial position) necessary for biofilm growth independently of the substrate surface stiffness. In contrast, the total length travelled by bacteria (diffusion coefficient) varied positively with surface stiffness but not with biofilm growth. The softest, hydrated HA, the least colonized surface, revealed the least diffusive and the least free-moving bacteria. This finally shows that customizing surface elasticity and hydration together is an efficient means of affecting bacterial mobility and attachment to the surface, and thus designing biomedical surfaces to deter biofilm growth.

Keywords: Surface stiffness; hydration; polydimethylsiloxane (PDMS); hyaluronic acid; biofilm; bacterial mobility; protein patterns

1. Introduction

Contamination of medical surfaces by bacteria is inextricably linked to many infections in clinical practice, leading to increased use of antibiotics and the subsequent emergence of antibiotic-resistant bacteria [1,2]. These causal bacteria are also known to form difficult-to-remove biofilms on medical surfaces; thus, the need to develop materials that inhibit bacterial colonization on medical surfaces is of utmost priority [3]. In biofilm formation, pioneer bacteria attach to the surface of materials, form colonies, and produce a protective polymer matrix composed of polysaccharides and other biomolecules. Biofilms are typically highly challenging to eradicate, primarily because of the limited drug diffusion in their extracellular matrix and the physiological states (resistance and dormancy) that these bacteria can switch to protect themselves [4].

Surface mechanical properties emerged some ten years ago as a potential tool for controlling the colonization of biomedical materials by bacteria [5-8]. Indeed, bacteria can sense the mechanical properties of their environment and quickly and appropriately respond to them [9,10]. The stiffness of a host's extracellular

matrix [11] or a material's surface in contact with bacteria modulate the interactions between the bacteria and their environment [5-8].

There are two uncertainties limiting the exploitation of surface mechanical properties to prevent biofilm formation on medical devices. First, recent studies on polydimethysiloxane (PDMS), polyelectrolyte multilayers (PEMs), poly(ethylene glycol) dimethacrylate (PEGDMA) or on agar hydrogel surfaces showed that the influence of stiffness on bacterial adhesion differs according to substrate; the stiffer PDMS materials are [12,13], or the softer hydrogels or PEMs are, the less bacteria adhered [6-8,14,15]. The reason for this marked difference is still unclear as these observations could be due to the presence or absence of the culture medium used, variations in the bacterial species, and to strong differences in the material hydration (typically observed between PDMS and agar hydrogels). Secondly, the biological actors and pathways regulated in this type of material-bacteria interface are still unknown, but they are necessary to elucidate the bacterial mechanosensing and the underlying mechanisms in the expansion or prevention of bacterial populations on soft and stiff surfaces.

In this study, we determined the behavior and proteome of *Escherichia coli* (*E. coli*) placed in contact with both hydrated and non-hydrated surfaces of differing elasticity. Short- and longer-term colonization (i.e. biofilm formation) were both considered as well as the capacity of the bacterial population to expand on the surface through individual bacterial mobility. We conducted this study on PDMS and on hyaluronic acid-based (HA) materials. PDMS elastomers are non-degradable synthetic polymers commonly used to design medical devices and implants, such as breast implants, contact lenses or catheters, while HA hydrogels have been used more recently as biomaterials for dermal wound repair and as scaffolds in tissue engineering [16,17]. The HA and PDMS materials were designed to have Young's moduli ranging from around 10 Pa to a few kPa, and from a few kPa to hundreds of kPa, respectively. The stiffest HA and the softest PDMS materials were adapted to provide similar Young's moduli (a few kPa) to allow direct comparison between these materials. The material's ability to store aqueous liquids (water content measurement) was determined as an index of hydration capacity. The materials were also characterized in terms of their surface chemistry, hydrophobicity/hydrophilicity, topography, and elasticity to describe the surface parameters that directly impact bacterial adhesion. Adhesion, retention (i.e. the fraction of adhered bacteria retained after the creation of an air-surface interface), mobility of the sessile bacteria, as well as further biofilm formation were evaluated *in situ* by fluorescence confocal microscopy during the first and longer colonization period on the hydrated and non-hydrated materials of differing surface elasticity. The protein patterns of the adhered bacterial cells were determined by a quantitative proteomic approach.

2. Materials and Methods

Synthesizing the PDMS materials. PDMS materials were prepared using the SYLGARD™ 184 Silicone Elastomer Kit (Dow Corning Corporation). The material's stiffness was adjusted by varying the curing agent-to-base mass ratio from 1:80 ("PDMS-9kPa") to 1:5 ("PDMS-574kPa"). For each ratio, the elastomer base and curing agent were thoroughly mixed. The mixture was poured into a plastic cup, cured at 120 °C for 20 min, and incubated at room temperature for 24 h to drive complete polymerization. The polymerized elastomer was cut into 8 mm diameter disks using a circle cutter previously sterilized under UV for 30 min. The synthesized PDMS materials were stored at room temperature until use. Samples were from 1.5 mm to 2.0 mm thick (measured with a caliper). The chemical structure of the PDMS polymer is illustrated in Figure 1A, and images of the samples are shown in Supplementary Materials (Figure S1A).

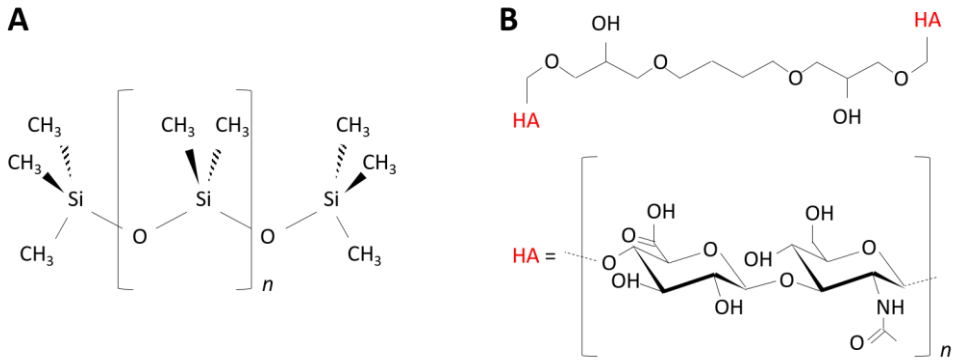

Figure 1. Chemical structures of the poly(dimethyl)siloxane (PDMS) (A) and hyaluronic acid (HA) (B) polymers prepared in this study.

Synthesizing the HA hydrogel materials. Hyaluronic acid (HA) hydrogels were made with the 1,4-butanediol diglycidyl ether (BDDE) crosslinker, as described in a previous work [18]. Briefly, a 0.038 mM solution of HA (Lifecore Biomedical, USA; MW = 823 kDa) in NaOH (0.25 M) was mixed with 10 % and 30 % BDDE (v/v) to prepare the "HA-44Pa" and "HA-2kPa" materials, respectively. The mixture was poured into a 35 mm diameter Petri dish and allowed to crosslink at 37 °C for 72 h. The HA hydrogel was further cut into 8 mm disks using a circle cutter, previously sterilized with UV for 30 min. HA hydrogel samples were stored at 4 °C until use. Samples were about 2.0 mm thick at room conditions. The chemical structure of the HA hydrogel polymer is illustrated in Figure 1B, and images of the samples are shown in Supplementary Materials (Figure S1B).

Characterizing surface chemistry. The chemical composition of the topmost sample surfaces was determined using X-ray photoelectron spectroscopy (XPS) on a VG SCIENTA SES-2002 spectrometer equipped with an Al Kα monochromatic x-ray source (1486 eV) at a power of 420 W. XPS analysis was carried out under pressure of 10^{-9} mbar on areas of about 4 mm × 6 mm and at a pass energy of 500 eV for survey spectra and 100 eV for high-resolution spectra of carbon (C1s), oxygen (O1s) and silicon (Si2p). The peaks were fitted by Gaussian-Lorentzian functions using XPS-CASA software (casaXPS software 2.3.18 Ltd., Teignmouth, UK) after subtracting a Shirley background [19]. The atomic concentration analysis was based on the integrated peak area of each component and took into account the sensitivity factor, mean free pathway of an electron, and the transmission function of the analyzer. The binding energies were set based on information in literatures and all components were referenced according to the CHx/C-C component at 285.0 eV [20,21].

Characterizing surface topography. The surface topography of the PDMS and HA materials was analyzed using atomic force microscopy (AFM). AFM images were acquired in contact mode with a Bioscope AFM microscope (Veeco, Santa Barbara, USA) and a ScanAsyst® Fluid cantilever probe (Bruker AFM Probes) in silicon nitride with a reflective gold back side coating (spring constant: 0.7 N/m; triangular geometry; tip radius: 20 nm). The analysis was performed with a resolution of 512 × 512 pixels at a scan rate of 0.5 Hz. Material samples were immersed in phosphate-buffered saline solution (PBS) during analysis. One 20 µm × 20 µm zone was acquired per sample. AFM images were treated and the mean surface roughness (*Sa*) was calculated using Gwyddion® software [22].

Characterizing surface wettability. Surface wettability was determined by measuring water contact angles in static mode. Measurements were made using an Attension® Theta tensiometer (Biolin Scientific, Sweden). The sessile drop method was used to evaluate the contact angle at equilibrium (θ) of a 5 µL distilled water drop on the sample surface. Briefly, the drop was deposited on the material surface via a 0.7 mm inner diameter needle, and 1 min long videos were recorded by a CCD camera (1 image / 0.07 s) from the moment the water

droplet hit the material until it reached a stable shape, i.e., when equilibrium was reached. The contact angle was evaluated at this point. Values of θ were extracted from the images using numerical fits of the droplet shape based on the Young-Laplace model [23]. The results obtained are presented as the mean ± standard deviation of at least two measurements per material. The material surfaces were qualified as either hydrophobic (when $\theta > 90°$) or hydrophilic (when $\theta < 90°$) [24]. For HA hydrogels, precise measurement of contact angles was not possible due to the fast absorption of the water drop by the material.

Characterizing material hydration. Hydration of PDMS and HA materials was evaluated by measuring their water content after full hydration. Material samples were weighed before immersion (w_1) in distilled water for 24 h at room temperature. After this period, the excess water was removed very delicately with absorbent paper, and the samples were weighed again (w_2). They were then dehydrated in an oven at 30 °C for 72 h and weighed (w_3) for a third time. Drying time t_0 was chosen as the minimal duration needed to measure constant w_3 values for $t > t_0$. Drying was thus considered to be complete at this time t_0. The water content was calculated according to Equation 1. Measurements were repeated on three independent samples for each material. The material hydration results are presented as mean ± standard deviation of the three measurements.

$$Water\ content\ (\%) = 100 \times \frac{w_2 - w_3}{w_2} \quad (1)$$

Characterizing surface elasticity. The elasticity of the material's surface was studied using a Chiaro® nano-indenter (Optics11 Life, The Netherlands). Nanoindentation analysis was performed in the liquid phase (M63 medium [25]) according to the ferrule top indentation method [26]. The indentation of a spherical glass probe in the material tested was calculated with interferometric detection. The spring constant of the cantilever and the radius of the spherical probe were selected to match the surface properties (2.90 N/m and 23.5 μm for PDMS-574kPa; 0.53 N/m and 25.5 μm for PDMS-9kPa; 0.53 N/m and 25.5 μm for HA-2kPa; 0.027 N/m and 24.5 μm for HA-44Pa). Measurements were made on a grid pattern and with 20 μm between two successive indentation locations. The approach velocity was fixed at 5 μm s^{-1}. The measurements were repeated 25 times, 29 times, 28 times and 25 times on PDMS-574kPa, PDMS-9kPa, HA-2kPa and HA-44Pa materials, respectively. Young's moduli (E) were calculated using the Hertz model [27]. Results are shown as mean ± standard deviation.

Bacterial strains and growth medium. Microbiological experiments were conducted with the *E. coli* K-12 SCC1 strain [28] (purchased by Prof. Chun Chau Sze, Nanyang Technological University, Singapore), which constitutively expresses the green fluorescent protein (GFP), produces colonic acid and flagella, and forms biofilms. Bacteria from a -80 °C frozen stock were grown overnight at 30 °C on lysogeny broth (LB) (Difco™, US) agar plates. Then, a colony was suspended in LB medium and incubated at 30 °C overnight. 3 mL of the first culture were then added to 27 mL of fresh LB. After 3 h of incubation at 30 °C, the suspension was centrifuged at 3000 rpm for 20 min, and the bacterial pellet was re-suspended in M63G medium [25] for experiments with alive bacteria. For experiments with killed bacteria, the bacterial pellet was re-suspended in a solution of 3.7% (w/v) paraformaldehyde in PBS. The suspension was homogenized by vortexing and agitating for 1 min and 3 h respectively at room temperature. The suspension was then centrifuged at 3000 rpm for 20 min and resuspended in M63G. 100 μl of this suspension was spread on LB agar Petri dish and incubated at 30 °C for 24 h to verify bacterial cell death. The optical density of the alive or killed bacteria suspensions (i.e. absorbance at 600 nm) was adjusted to 0.01, corresponding to approximatively 5×10^6 bacteria/mL.

Bacterial culture and sample preparation for adhesion, retention, and mobility analyses. Material samples were set on to a glass coverslip with a dot of biocompatible glue, placed in a 12 mm diameter home-made sample-holder (Figure S2) and immersed with 1.5 mL of *E. coli* K-12 SCC1 suspension before incubation at 30 °C for 3 h. Glass coverslips were used as internal controls in each experiment. For adhesion and mobility analyses, planktonic

bacteria were removed using a washing procedure based on dilutions in order to avoid any dewetting of the sample surface and the related risk of driving away sessile bacteria due to the action force applied by the triple line [29]. 500 µL of the bacterial planktonic suspension were therefore carefully removed and replaced by 500 µL of fresh M63 medium (i.e., M63G without glucose). This was repeated three times to reach an OD value for the supernatant removed of about 0. For the analysis of retention (i.e. the fraction of adhered bacteria retained after the creation of an air-surface interface), the washing procedure was performed as follows: all the supernatant (1.5 mL) was removed without contact with the material; 500 mL of fresh M63 medium was then delicately added and removed. This procedure was repeated three times.

Bacterial culture and sample preparation for biofilm (longer-term colonization) analysis. Samples were prepared as described above for adhesion, retention, and mobility analysis but after a longer culture time (72 h). Briefly, material samples, set on to a glass coverslip with a dot of biocompatible glue and placed in a 12 mm diameter home-made sample-holder were immersed with 1.5 mL of *E. coli* K-12 SCC1 suspension before incubation at 30 °C for 3 h. Planktonic bacteria were then removed using the same washing procedure as for the adhesion analysis. Samples were further incubated under static conditions for the remaining time (69 h).

Microscopy analysis. The adhesion, retention, and mobility of sessile bacteria as well as biofilms were analyzed with a confocal laser scanning microscope (CSLM) (LSM710, Zeiss, Germany) equipped with a 50× objective (Objective LD EC Epiplan-Neofluar 50×/0.55 DIC M27; working distance = 9.1 mm). A 488 nm excitation wavelength laser was used to excite the GFP produced by *E. coli* K-12 SCC1 and to make it possible to detect the bacterial cells. The fluorescence emitted was thus collected from 493 nm to 578 nm for adhesion, retention, and mobility analyses, or from 493 nm to 544 nm for biofilm analyses. For biofilm analysis, the collected range of wave length was reduced to allow the staining of the biofilm matrix with another fluorescence dye (Texas Red™ concanavalin A; see below). For the adhesion and retention analyses, at least 5 images for each sample were taken *in situ* in the final washing medium. For the mobility analyses, at least 5 one-minute videos (1 image every 3, 4 or 5 s, depending on the experiment) were taken in the same conditions. For the biofilm analyses, the biofilm matrix was previously stained with Texas Red™ concanavalin A (ConA) (Invitrogen™), which selectively binds to α-mannopyranosyl and α-glucopyranosyl residues. The ConA powder was diluted in a 0.1 M sodium bicarbonate ($NaHCO_3$) solution to obtain a 2 mg/mL concentration, which was added to the final washing medium. The final ConA concentration was 125 µg/L. After 30 min of incubation at 30 °C in the dark, at least 5 3D-images (Z-stacks) were taken *in situ* in the final washing medium. The 561 nm excitation wavelength laser was used to excite the ConA. The fluorescence emitted by ConA was collected between 582 nm and 650 nm. The locations analyzed were determined randomly for all analyses. Each experiment was repeated at least 3 times. The number of adhered and retained bacterial cells was determined from the microscopy images with automatic counting of the individual cells using ImageJ® 2.0 software [30] and the Analyze Particles plugin. Cell tracking of sessile bacteria in the one-minute videos was done with the NIS-Elements Advanced Research Imaging software® (Nikon Group™) using the automated object tracking module. A list of the consecutive coordinates for the position of each bacterium during the one-minute video was generated. Further analysis of bacterial mobility was done using these data. The biovolume per surface unit corresponding to cell and matrix of the biofilm, that is GFP- and ConA-related biovolumes per surface unit, respectively, were extracted with the Comstat2® software and expressed in $\mu m^3/\mu m^2$ [31].

Data and statistical analysis. Statistical significance of the differences in adhered or retained bacteria numbers, as well as biofilm features (biomass), was determined with *t*-tests. The H_0 hypothesis ($\mu_1 = \mu_2$) was rejected for *p*-values < 0.05, *p*-values < 0.01 or *p*-values < 0.001 depending on the experiment (see figure captions). The raw data used for mobility analysis were the *E. coli* (x,y) positions at successive times. Only paths that could be followed over about 1 min (precisely 55, 57 or 76 s depending on the experiment) were selected. The analysis focused on the values of d_{net}, which is the net distance travelled by a bacterial cell from the first image (at $t = 0$

of the experiment) to the image observed at a given time t during the experiment (Figure 2). The experimental cumulative relative frequency F of d_{net}^2 was determined for each observation time on each sample.

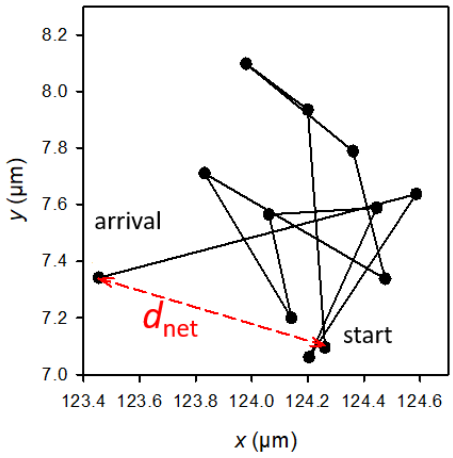

Figure 2. Example of the trajectory of a bacterium observed at a given t time of the experiment, and schematic definition of d_{net} (in red); the sum of the black segments gives the total length, d_{tot}, of the trajectory. Each dot corresponds to the position of the bacterium at the successive times from 0 to t (t from 0 to 55, 57 or 76 s according to the experiment).

If all bacteria had free Brownian motion with the same diffusion coefficient D, the complementary cumulative relative frequency, $\Phi = 1 - F$ would be a decreasing exponential function of d_{net}^2, i.e. $\Phi = \exp\left(-\frac{d_{net}^2}{4Dt}\right)$. In other words, as a general rule, when Φ is known, $\Phi(x_0)$ represents the probability of finding a value of $x \geq x_0$. In our observations, however, Φ was not a decreasing exponential function of d_{net}^2. We thus devised a model that assumed that the bacteria sampled by each experiment encompassed m subpopulations with homogeneous characteristics of motion. In each subpopulation, bacteria were considered as moving in a harmonic energy well, $U(r)$ (where r *is* the position of the bacterium referred to the well center), with characteristic radius (r_C) defined by $U(r_C) / k_B T = 1$, where $k_B T$ is the thermal energy (Equation 2). The movement is Brownian with diffusion coefficient D, but not exclusively due to thermal agitation; at a radial distance r from the center of the well, the bacterium experiences a restoring force as modeled by a Hooke spring. In these conditions, preliminary simulations made it possible to determine the dependence of $<d_{net}^2>$ on the parameters D and r_C, and on time t (Equation 3). This equation is similar to that found by Meijering *et al.* [32] because $<d_{net}^2>$ is the mean squared displacement (MSD) taken at the final observation time. The free Brownian motion is recovered when r_C tends toward infinity (Equation 4a), whereas $<d_{net}^2>$ tends toward a limit imposed by the well when t tended toward infinity (Equation 4b).

$$\frac{U(r)}{k_B T} = \left(\frac{r}{r_C}\right)^2 \quad (2)$$

$$< d_{net}{}^2 > = 2\, r_C{}^2 \left(1 - e^{-2Dt/r_C{}^2}\right) \quad (3)$$

$$\text{with } \lim_{r_C \to \infty} < d_{net}{}^2 > = 4\, D\, t \quad (4a)$$

$$\text{and } \lim_{t \to \infty} < d_{net}{}^2 > = 2\, r_C{}^2 \quad (4b)$$

It was then possible to calculate the function Φ of d_{net} for the m subpopulations according to Equation 5.

$$\Phi = \sum_{i=1}^{m} w_i\, e^{-d_{net}{}^2/<d_{net}{}^2>_i} \quad (5)$$

where $<d_{net}^2>_i$ depends on the (D_i, $r_{C,i}$) couple, and w_i is the relative weight of the i^{th} subpopulation (the weights are subject to the constraints $\sum_{i=1}^{m} w_i = 1$ and $w_i \geq 0$ for any i).

The same preliminary simulations also gave access to the expression of the mean total length, $<d_{tot}>$, of the trajectories following Equation 6.

$$< d_{\mathrm{tot}} > = \sqrt{\frac{\pi}{2}} \frac{t}{\Delta t} r_{\mathrm{C}} \sqrt{1 - e^{-2D\Delta t / {r_{\mathrm{C}}}^2}} \quad (6)$$

where t is the observation duration and Δt the time lag between the successive pictures.

The mean speed follows then merely by dividing $<d_{tot}>$ by the corresponding time t according to Equation 7.

$$< v > = \sqrt{\frac{\pi}{2}} \frac{1}{\Delta t} r_{\mathrm{C}} \sqrt{1 - e^{-2D\Delta t / {r_{\mathrm{C}}}^2}} \quad (7)$$

In the special case when $r_C \to \infty$, $<v>$ reduces to Equation 8.

$$< v >= \sqrt{\frac{\pi D}{\Delta t}} \quad (8)$$

The challenge was then to find the m triplets (D_i, $r_{C,i}$, w_i). To this end, an optimization method known as "simulated annealing" was used. The aim was to reduce, as much as possible, the sum (S) of the squares of the differences between the experimental Φ_{exp} and the computed one, Φ_{comp}. For a fixed number of subpopulations, m, and a starting initial "temperature", T_{ini}, the weight w_i corresponding to (D_i, $r_{C,i}$) of each of the m triplets is varied to reduce S. After a number of minimization trials, the temperature is lowered (e.g. by a factor of 1.05 until no new configuration could be accepted by the Metropolis criterion [33]. The process goes on until no further reduction of E can be achieved. The quantity E, which plays the role of energy, and the quantity called "temperature" are borrowed from the simulated annealing method first developed in statistical physics. Pre-processing of the experimental data and simulated annealing were performed with home-made computer codes written in Fortran®. From the triplet (D_i, $r_{C,i}$, w_i) a confinement index ($\rho_i \in [0,1]$) could be defined with Equation 9.

$$\rho_{\mathrm{i}} = \frac{<{d_{\mathrm{net}}}^2>_{\mathrm{i}}}{2\,{r_{\mathrm{C,i}}}^2} \quad (9)$$

for each of the m subpopulations.

Analysis of the whole proteome. *Protein extraction.* Proteomic analyses were carried out on cells adhered to the HA-44Pa and HA-2kPa, and PDMS-9kPa and PDMS-574kPa materials. HA and PDMS substrates were inoculated for 3 h and rinsed as described above. Adhered cells were delicately detached with a cell scraper. The scraped cells were removed from the cell scraper with fresh M63 rinses. Solution containing the cells was transferred into 1.5 mL Eppendorf tubes, which were centrifuged at 10000 rpm for 30 min. The supernatant was then removed, and the pellet was stored at -20 °C until analyzed. Proteins were extracted by two freezing cycles and sonication in a lysis buffer (7 M urea, 2 M thiourea, 4 % 3-[(3-cholamidopropyl) dimethylammonio]-1-propanesulfonate hydrate (CHAPS), 65 mM dithiothreitol (DTT), 25 mM Tris/HCl). Protein concentrations were determined using the Bradford assay [34].

Enzymatic digestion. Twenty micrograms of protein were mixed with SDS loading buffer (63 mm Tris-HCl, pH 6.8, 10 mm DTT, 2 % SDS, 0.02 % bromphenol blue, 10 % glycerol) and loaded on to an SDS-PAGE stacking gel (7 %). A short electrophoresis was performed (10 mA, 45 min and 20 mA, 2 h) to concentrate the proteins. After migration, the gels were stained with Coomassie Blue and unstained (50 % ethanol, 10 % acetic acid, 40 % deionized water). The protein band revealed from each fraction was excised, washed with water, and immersed in a reductive medium (5 mm DTT). Cysteines were irreversibly alkylated with 25 mm

iodoacetamide in the dark. Following washing steps in water, the gel bands were submitted to protein digestion with trypsin (1 μg per band), overnight at 37 °C, in ammonium bicarbonate buffer (10 mm, pH 8). Peptides were extracted with H_2O/CH_3CN/TFA mixtures (49.5/49.5/1) and dried. For each growth condition, three biological replicates were performed and two technical replicates were made for each of them (in total, 6 samples per condition were analyzed).

Tandem mass spectrometry. Peptides were analyzed using mass spectrometry. All experiments were performed on an LTQ-Orbitrap Elite (Thermo Scientific) coupled to an Easy nLC II system (Thermo Scientific). One microliter of sample (1 μL) was injected onto an enrichment column (C18 PepMap100, Thermo Scientific). The separation was performed with an analytical column needle (NTCC-360/internal diameter: 100 μm; particle size: 5 μm; length: 153 mm, NikkyoTechnos, Tokyo, Japan). The mobile phase consisted of H_2O/0.1 % formic acid (FA) (buffer A) and CH_3CN/FA 0.1 % (buffer B). Tryptic peptides were eluted at a flow rate of 300 nL/min using a three-step linear gradient: from 2 to 40 % of buffer B over 75 min, from 40 to 80 % of buffer B in 4 min and 11 min at 80 % of buffer B. The mass spectrometer was operated in positive ionization mode with capillary voltage and the source temperature set at 1.5 kV and 275 °C, respectively. The samples were analyzed using the collision induced dissociation (CID) method. The first scan (MS spectra) was recorded in the Orbitrap analyzer (Rs = 60,000) with the mass range *m*/*z* 400–1800. Then, the 20 most intense ions were selected for tandem mass spectrometry (MS^2) experiments. Singly charged species were excluded for MS^2 experiments. Dynamic exclusion of already fragmented precursor ions was carried out for 30 s, with a repeat count of 1, a repeat duration of 30 s and an exclusion mass width of ± 10 ppm. Fragmentation occurred in the linear ion trap analyzer at a collision energy of 35 eV. All measurements in the Orbitrap analyzer were performed with on-the-fly internal recalibration (lock mass) at *m*/*z* 445.12002 (polydimethylcyclosiloxane).

Protein quantification. A label-free experiment was performed as previously described by Obry *et al.*[35]. Briefly, after MS analysis, raw data were imported into the Progenesis LC-MS software (Nonlinear Dynamics, version 4.0.4441.29989, Newcastle, UK). For comparison, one sample was set as a reference and the retention times of all other samples within the experiment were aligned. After alignment and normalization, statistical analysis was performed for one-way analysis of variance (ANOVA) calculations. For quantitation, peptide features presenting a *p*-value and a q-value of less than 0.05, and a power of more than 0.8, were retained. MS/MS spectra from selected peptides were exported for peptide identification with Mascot (Matrix Science, version 2.2.04) against the database restricted to *E. coli* K12 MG1655 from NBCI. Database searches were performed with the following parameters: 1 missed trypsin cleavage site allowed; variable modifications: carbamidomethylation of cysteine and oxidation of methionine. Mass tolerances for precursor and fragment ions were set at 5 ppm and 0.35 Da, respectively. False discovery rates (FDR) were calculated using a decoy-fusion approach in Mascot (version 2.2.04). Identified peptide-spectrum-matches with a −10logP value of 20 or higher were kept at an FDR threshold of 5 %. Mascot search results were imported into Progenesis. For each condition, the total cumulative abundance of the protein was calculated by summing the abundances of peptides. Proteins identified with less than 2 peptides were discarded. Only the proteins with a 2-fold variation in their average normalized abundances between growth conditions were retained.

3. Results and Discussion

The HA (from (44 ± 16) Pa to (2.2 ± 0.6) kPa)) and PDMS (from (9 ± 2) kPa to (574 ± 11) kPa) materials cover a wide range of surface elasticity as well as opposite hydration properties (Figure 3A and Table S2). As expected, the Young's modulus *E* (analyzed with nanoindentation) increased with increasing crosslinking for both materials. It is important to note that the stiffest HA (HA-2kPa) and the softest PDMS (PDMS-9kPa) revealed a similar Young's modulus. This trend was confirmed by the bulk properties evaluated by rheometry (Figure

S3), although a quantitative difference was expected due to the difference in stimulation between both methods (perpendicular to the surface for the nanoindentation or oscillating, shear stress for rheometry). . Rheometry also revealed that, as expected, PDMS with 1:40 and 1:20 curing-to-base ratio had intermediate stiffness (10.2 ± 0.7 and 34 ± 9) (Figure S3F). Furthermore, consistent with literature [36], elastic behavior predominated in all materials except for PDMS-9kPa, which displayed a significant viscous behavior, as previously reported by Valentin et al. [37]. However, increasing crosslinking does not change the viscous component in HA materials, whereas it only weakly increases in PDMS materials. It is important to note that nanoindentation rather than rheology can effectively detect the surface elasticity sensed by bacteria when in contact with a material's surface. Therefore, in the following sections, we describe surface elasticity using the Young's modulus *E* obtained by nanoindentation.

As expected, water content was low for the PDMS materials, varying from about 1 % to 5 %. On the contrary, the HA materials displayed typical hydrogel behavior, with water content of about 97 % and more than 99 % for HA-2kPa and HA-44Pa, respectively. The hydrophobic or hydrophilic characters were in accordance with those expected from the material's hydration capacity. The values of the water contact angle θ at equilibrium were less than 10° on both HA surfaces (they could not be measured more accurately due to rapid water absorption in the hydrogel materials), whereas θ values showed an expected hydrophobic nature for both PDMS-9kPa and PDMS-574kPa (115 ± 1° and 114 ± 2°, respectively) [13,38-40].

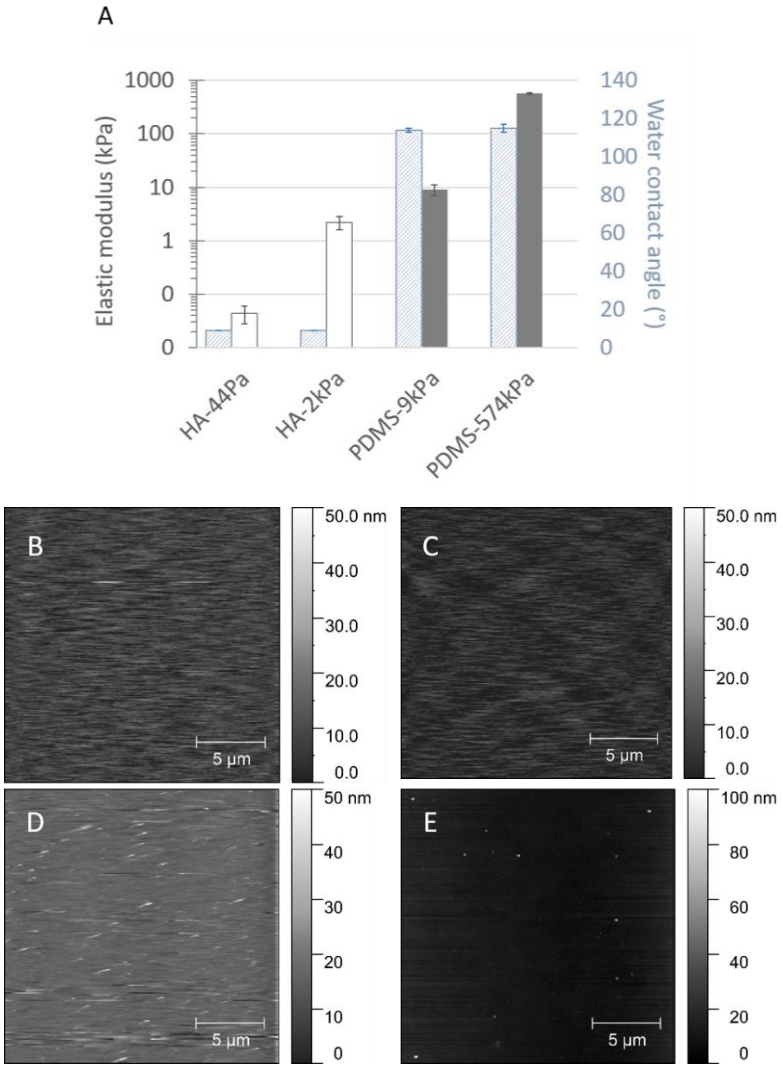

Figure 3. Elastic, hydrophobic and topographic properties of the material surfaces, displayed as the Young's moduli E and the water contact angle at equilibrium (A), and as AFM micrographs of HA-44Pa (B), HA-2kPa (C), PDMS-9kPa (D) and PDMS-574kPa (E) materials. Mean Young's moduli were determined by nanoindentation for each material type (average and standard deviation from 17 to 29 measurements).

Aside from elasticity, surface topography and chemistry can directly act bacterial adhesion. Herein, topography is quantified by the roughness, which gives a general view of the surface, and AFM images complete the description regarding texture and morphology. Sa values were less than 4 nm on all the materials (2.9 nm, 2.8 nm, 3.8 nm and 2.5 nm for HA-44Pa, HA-2kPa, PDMS-9kPa and PDMS-574kPa materials, respectively) and only rare peaks were present (maximum height of about 30 nm and 90 nm on HA and PDMS materials, respectively) (Figures 3B-E). Chemistry is described by the chemical groups that may be involved in specific chemical interactions with receptors on the bacterial surface and by the hydrophobicity/hydrophilicity, which may hamper the contact of a bacterium with the surface if a layer of water molecules is present at the material surface, or allow hydrophobic interactions between the bacterial outer surface and the material surface on hydrophobic surfaces. Surface charge was not considered, since it cannot have significantly impacted bacterial adhesion in a culture medium of high ionic strength (about 150 mM for LB and M63G). Electrostatic interactions between the charges carried by the bacterium and the material surface are strongly reduced in such ion-rich media as illustrated by the Debye length which was found to be as small as 0.8 nm [41,42].

3.1. E. coli adhesion, retention and biofilm growth have an opposite correlation with stiffness on HA and PDMS surfaces

Bacterial adhesion (i.e. measured after 3h of culture *in situ* without retrieval of the liquid environment) and retention (i.e. measured after surface retrieval from the liquid) increased significantly as PDMS surface elasticity decreased. Although the results on HA surfaces suggested an opposite trend, an intermediate stiffness value between HA-44Pa and HA-2kPa would be required to conclude a monotone relationship. By adhesion tests, we showed that adhesion rises by a factor of 1.8 on HA surfaces when E increases from 44 Pa to 2.2 kPa, whereas it rises by a factor of 1.3 on PDMS surfaces when E decreased from 574 kPa to 9 kPa (Figure 4 and Figure S4). Retention followed the same trends on both PDMS and HA materials (Figure 4A). However, cell numbers were reduced by more than 50% in comparison with adhesion tests. This was probably caused by the shear stress applied to sessile bacteria by the triple line of the dewetting front created by retrieval of the liquid during the retention test (Figure S5) [43-45]. After 72 h PDMS-574kPa and HA-44Pa were less colonized than PDMS-9kPa and HA-2kPa, respectively, demonstrating that the general trend observed at 3 h was maintained (Figure 4B). However, PDMS-9kPa and HA-2kPa materials were similarly colonized by GFP-producing cells after 72 h of culture, while significantly fewer bacteria were adhered on HA than on PDMS materials after 3 h. The production of polymeric matrix also depended on the material: the matrix amount was much higher on PDMS-9kPa than on the HA-2kPa material, and it was almost completely absent on the HA-44Pa material. These results indicate that variations in surface elasticity and surface hydration result in variations in biofilm and act at several key-stages of its formation: 1) bacterial adhesion, 2) growth of the cell population, and 3) production of the polymeric matrix.

A

	HA-44Pa	HA-2kPa	PDMS-9kPa	PDMS-574kPa
E	44 ± 16 Pa	2.2 ± 0.6 kPa	9 ± 2 kPa	574 ± 11 kPa
G'	154 ± 53 Pa	2.3 ± 0.8 kPa	6 ± 2 kPa	147 ± 48 kPa
Water content	> 99%	97%	5%	1%
Θ	< 10°	< 10°	115 ± 1°	114 ± 2°

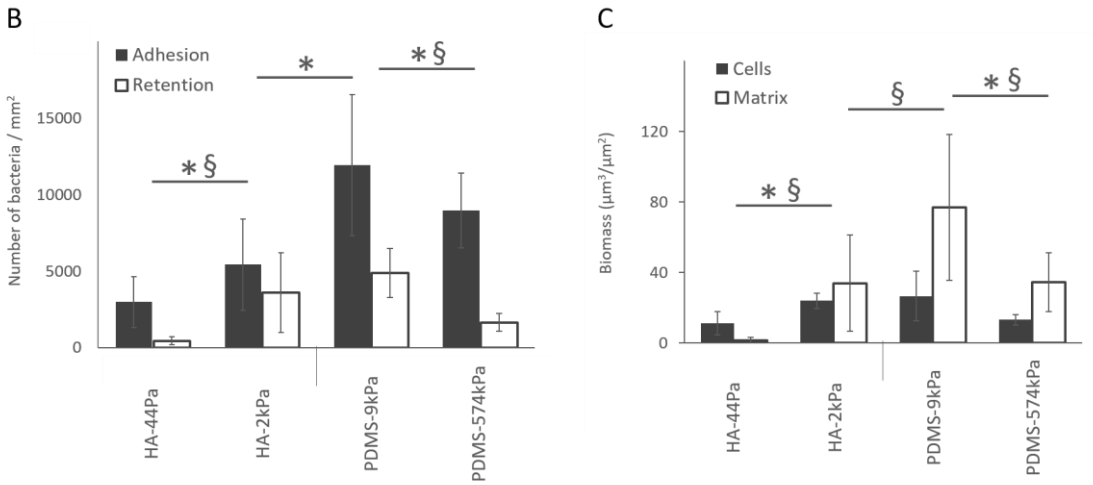

Figure 4. Bacterial adhesion, retention, and biofilm formation on the HA and PDMS materials. (A) Summary of the main properties of HA-44Pa, HA-2kPa, PDMS-9kPa and PDMS-574kPa materials; *E*, *G'* and θ are Young's modulus, elastic modulus and contact angle, respectively. (B) Adhesion (gray) and retention (white) after 3 h of culture, as determined on the micrographs (Syto9® staining). *,§: significant difference in adhesion and retention, respectively (p-value < 0.05). (C) Bacterial cell biomass and matrix amount of biofilms formed after 72 h of culture, as determined on the micrographs (Syto9® and Texas Red® concanavalin A stains, respectively). *,§: significant difference in cells and matrix quantity, respectively (p-value < 0.05).

In the literature (Table S1), results obtained after retention assays show similar trends on PDMS materials as in the present study [12,46]. Only a few works have considered bacterial adhesion rather than retention. They report comparable numbers of bacteria on soft and stiff PDMS [40,47] or even slightly lower on the softest compared to the stiffest surface [48]. These differences in the reported results are most probably caused by the conditions for washing the samples and harvesting the bacterial cells after the culture on the surfaces, aside from differing bacterial cells, culture medium, cell density for inoculation, and the methods used to count bacteria. To our knowledge, results of the bacterial colonization on HA hydrogels of differing elasticity have never been published. Reported data concern hydrogels made of agarose [6,14,15] and other hydrated materials based on polyethylene glycol [15,49,50], poly(N-isopropylmethacrylamide) [51] or polyelectrolytes [7], sometimes derived from HA [8]. Apart from Wang *et al.* [50], all authors concluded there was a decrease in bacterial adhesion or retention with decreasing material elasticity (Table S1), in agreement with the present study. Wang *et al.* reported an opposite trend on polyacrylamide hydrogels with elasticity values of less than 1 kPa [50]. However, the significant difference in surface topography of the 17-Pa PAAm and 654-Pa PAAm materials used in their work probably impacted the retention of bacteria on the surface. In the present study, differences in material surface chemistry and topography are not expected to directly modulate bacterial adhesion. Indeed, PDMS and HA substrates had a similar flat topography in relation to the size of a bacterium,

which did not significantly change with the degree of crosslinking (Figures 3B-E). According to the literature, it is fair to assume that such topography is unlikely to cause significant inter-sample variations in bacterial adhesion and retention [52]. Furthermore, the variation in the degree of crosslinking between soft and stiff materials did not profoundly change the surface chemistry at the extreme surface of either the HA or PDMS materials (Figure 1). However, surface chemistry differed, as expected, between these two materials (Table 1 and Figure S6). Binding energies attributed to C-Si, O-Si bonds and silicon oxides (SiO_2 or SiO_4) were detected on PDMS materials, whereas C-C, C-H, C-O and C=O bonds were detected on HA hydrogels. This difference cannot directly result in a difference in bacterial adhesion since the chemical groups present at the surface of PDMS and HA are not specific ligands of the bacterial membrane [53,54]. However, it can indirectly lead to differences due to the resulting surface charge and hydrophobic character. As previously noted, the difference in surface charge cannot have significantly impacted bacterial adhesion in a culture medium of high ionic strength. However, the hydrophobic or hydrophilic property that the detected groups conferred on the surface probably had an impact on bacterial adhesion. The values of the water contact angle θ at equilibrium (less than 10° on HA surfaces and about 115° on PDMS surfaces) are consistent with a significant difference in adhesive properties between highly hydrophilic HA and hydrophobic PDMS surfaces. Water molecules present at the HA material surface probably impede the attachment of bacteria to the surface [55,56] whereas hydrophobic surfaces such as PDMS materials may be more favorable to attractive interactions between the surface and a bacterium [57,58]. Therefore, on PDMS, bacterial adhesion decrease when stiffness increases can be considered the actual effect of surface elasticity. On the contrary, the effect of surface hydration may offset the effect of surface elasticity on HA materials. The hydration of HA surfaces in comparison to PDMS also probably hinders the production of the extracellular polymer matrix or its attachment to the surface. Indeed, water molecules at the hydrophilic surface may hamper bacterial sensing of the surface and, subsequently, prevent the physiological change from planktonic to sessile [59]. The polymer matrix may also have insufficient tethers and therefore insufficient stability to remain on such a hydrated surface [56].

Table 1. Chemical composition of the PDMS and HA material surfaces as evaluated by High-Resolution XPS analysis.

	Peak	Component	Position (eV)	Atomic %	
				PDMS-9kPa	**PDMS-574kPa**
	C1s	C-Si	284.3	44	46
PDMS	O1s	Si-O	532.0	28	27
	Si2p	Si $2p_{3/2}$ SiO	101.8	22	24
		Si $2p_{3/2}$ SiO_4 SiO_2	103.2	6	4
				HA-44Pa	**HA-2kPa**
	C1s	C-C C-H	285.0	15	25
HA		C-O	286.5	49	45
		C=O	288.0	3	2
	O1s	CO	532.9	34	29

Finally, the difference in bacterial adhesion and retention on HA and PDMS surfaces with different elasticity has most probably resulted from the difference in elastic character, which was offset by hydrophilic character

on the HA surface. These surface properties may have caused differences in bacterial biology, in particular regarding surface sensing and tethering to the material surface [60].

3.2. MscS and FimA abundances vary with surface stiffness and surface hydration

We next determined whether these combinations of surface stiffness and surface hydration may regulate protein expression in *E. coli*. (Figure 5A). On HA materials, MscS and eight other proteins (Lon, RpoS, GatC, SecYEG, RplV, RpmC, RplB, RhlE; Table 2) were more abundant on the HA-44Pa than on the HA-2kPa surface, among 900 proteins. Five proteins were more abundant on the HA-2kPa than on the HA-44Pa surface (DnaK, PykF, Eno, AldA, RpsA). On PDMS materials, FimA and seven other proteins (AdhE, Lpp, PolA, LacZ, FtsY, Mog, TopA; Table 3) were more abundant on the PDMS-9kPa than on the PDMS-574kPa surface among about 1000 proteins. Two proteins were in higher abundance on the PDMS-574kPa than on the PDMS-9kPa surface (CysE and PurD). Furthermore, four proteins were found accumulated on both HA-2kPa and PDMS-9kPa compared to HA-44Pa and PDMS-574kPa surfaces, respectively (Table 4A). However, their maximum fold change (MFC) values were low except for AdhE protein on PDMS surfaces. All these data point out an alteration of the protein patterns according to the materials.

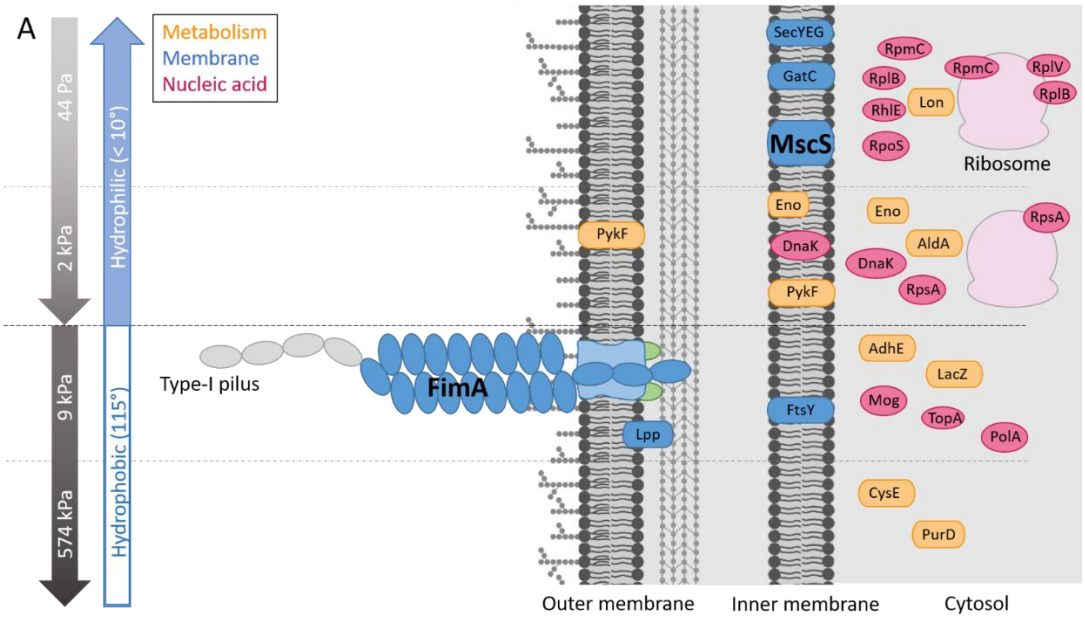

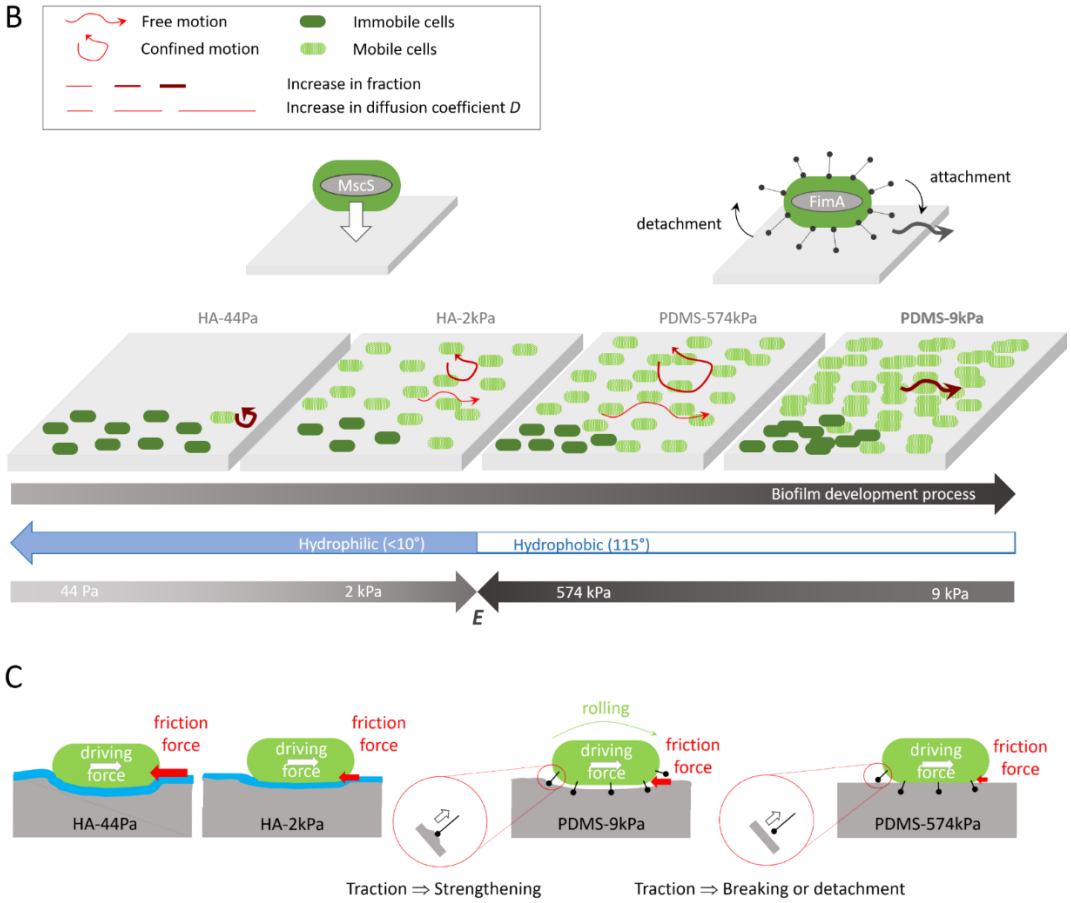

Figure 5. Summary of the influence of PDMS and HA surface elasticity and surface hydration levels on (A) protein abundance in the *E. coli* proteome as determined by proteomic analyses (the highest abundances are shown) and (B) the mobility and biofilm development of the *E. coli* sessile populations, as suggested by the integrated results, and (C) hypothesis of the role of friction forces and pili-tethers in the bacterial mobility on the surfaces.

Table 2. Differentially expressed proteins in *E. coli* sessile cells on HA-44Pa and HA-2kPa materials. MFC: Max Fold Change.

Function		Name	Highest condition	MFC
Metabolism	Protein quality control	Lon Lon protease	HA-44Pa	19.7
	Dehydrogenase activity	AldA Lactaldehyde dehydrogenase	HA-2kPa	7.8
	Glycolytic process	Eno Enolase	HA-2kPa	5.3
	Glycolytic process	PykF Pyruvate kinase I	HA-2kPa	5.2
	Galactidol metabolic process	GatC PTS system galactitol-specific EIIC component	HA-44Pa	5.6
Membrane	Translocation	SecYEG Protein translocation channel SecYEG	HA-44Pa	17.1
	Mechanosensitive channel	MscS Small-conductance mechanosensitive channel	HA-44Pa	5.0

Nucleic Acid	DNA	DnaK Chaperone protein DnaK	HA-2kPa	17.6
	rRNA	RplV 50S ribosomal protein L22	HA-44Pa	6.3
		RpmC 50S ribosomal protein L29	HA-44Pa	5.2
		RplB 50S ribosomal protein L2	HA-44Pa	5.2
		RpoS RNA polymerase sigma factor RpoS	HA-44Pa	5.1
		RpsA 30S ribosomal protein S1	HA-2kPa	5.7
		RhlE ATP-dependent RNA helicase RhlE	HA-44Pa	6.0

Table 3. Differentially expressed proteins in *E. coli* sessile cells on PDMS-9kPa and PDMS-574kPa materials. MFC: Max Fold Change.

Function		Name	Highest condition	MFC
Metabolism	Carbon utilization, Ethanol biosynthetic process	AdhE Aldehyde-alcohol dehydrogenase	PDMS-9kPa	4.0
	Cysteine biosynthesis	CysE Serine acethyltransferase	PDMS-574kPa	4.0
	Molybdenum-cofactor biosynthesis	Mog Molybdopterin adenylyltransferase	PDMS-9kPa	2.6
	Lactose catabolic process	LacZ Beta-galactosidase	PDMS-9kPa	3.2
	IMP biosynthetic process	PurD Phosphoribosylamine–glycine ligase	PDMS-574kPa	2.9
Membrane	Pilus organization and cell adhesion	FimA Major type 1 subunit fimbrin (pilin)	PDMS-9kPa	15.0
	Protein targeting to membrane	FtsY Signal Recognition particle receptor	PDMS-9kPa	2.7
	Lipid modification, periplasmic space organization	Lpp Major outer membrane lipoprotein	PDMS-9kPa	2.5
Nucleic Acid	DNA replication, damage, and repair	PolA DNA polymerase I	PDMS-9kPa	4.9
	DNA topological change	TopA DNA topoisomerase I	PDMS-9kPa	4.6

Specifically, one remarkable protein in high abundance on HA-44Pa was MscS, a mechanosensitive channel of small conductance. MscS is known as a membrane tension sensor [61]. It opens in response to stretch forces in the membrane lipid bilayer and is believed to be sensitive to mechanical deformation of the cell wall induced by surface contact. This triggers surface-specific cellular responses. On HA-44Pa, bacteria probably sense mechanical characteristics using MscS channels as they can do in a liquid environment [10,62]. This may be possible thanks to the high softness and hydration of this material, which might provide adequate stimuli for

MscS channels. Furthermore, RpoS, overproduced on HA-44Pa, is associated with the transition to the stationary state at the beginning of bacterial adhesion to a surface [63], and Lon protease regulates bacterial motility during this type of transition in several species [64,65]. Their overproduction on HA-44Pa suggests that bacteria are in a very early stage of adhesion on this surface. In contrast, the higher abundance of DnaK observed on HA-2kPa is consistent with a more advanced stage of bacterial adhesion on this surface, as shown by the bacterial adhesion and biofilm formation assays (Figure 4). DnaK is associated with the production of curli [66], which are necessary for bacteria to tether themselves to surfaces and further strengthen biofilms [67]. It should be noted that proteins in the curli appendages were not identified in the proteomes. This may result from low production of curli by the bacteria, but also from the low solubility of such amyloid fibers [68], which may lead to their removal during sample preparation prior to mass spectrometry analysis. Thus, the protein production is consistent with the initiation or formation of biofilms on both HA surfaces, but surface stiffness of the HA-2kPa positively regulates the production of proteins favorable to adhesion compared to the HA-44Pa. As a consequence, adhesion and further biofilm production are probably delayed on the HA-44Pa compared to the HA-2kPa surface, in agreement with the quantity of biofilm measured on these surfaces (Figure 4).

Several proteins in higher abundance on PDMS-9kPa are also involved in biological processes related to biofilm formation. Thus, overproduction of FimA is related to higher production of Type-1 pili, which is an appendage used by *E. coli* to attach to abiotic surfaces [69,70] (see SEM micrographs of *E. coli* SCC1 producing pili in Figure S7) and is associated with high adhesion and biofilm formation. Interestingly, Type-1 pili are also sensitive to changes in the bacterial mechanical environment [71] and allow bacteria to attach to surfaces in a force-dependent, so-called "catch-bond", manner [72]. Production of AdhE, a multifunctional and key metabolic enzyme in bacterial physiology and pathogenicity, and Lpp, a major outer membrane protein of *E. coli*, are also positively correlated with biofilm formation [73,74]. In particular, Lpp protein is linked to CsgA expression [74], which is the major subunit of curli. In contrast, the higher abundance of CysE on PDMS-574kPa is consistent with the observed limitation of biofilm growth. Indeed, this enzyme has been associated with the inhibition of *E. coli* biofilm formation [75]. Thus, like HA surfaces, PDMS surfaces displayed protein production consistent with the initiation or formation of biofilms. However, surface stiffness of the PDMS-574kPa negatively regulates the production of proteins favorable to adhesion compared to the PDMS 9kPa. As a consequence, the biofilm formation process progressed probably with a delay on the PDMS-574kPa compared to the PDMS-9kPa surface, in agreement with the quantity of biofilm measured on these surfaces (Figure 4). Furthermore, the characterization of lower amount of FimA on the HA surfaces than on PDMS-574kPa surface (Table 4B) confirms that bacterial adhesion was just starting on HA surfaces, whereas it was at a more advanced stage on this PDMS surface.

Table 4. Examples of proteins differently expressed on HA and PDMS materials. (A) Four proteins were significantly less expressed on both HA-2kPa and PDMS-9kPa (p-value < 0.05) compared to HA-44Pa and PDMS-574kPa respectively; adhE is a protein positively correlated to biofilm formation, whereas the other proteins could not be related to bacterial adhesion or biofilm formation. (B) FimA, the main sub-unit of Type-1 pili located in the outer cell membrane, was identified on HA and PDMS materials. On PDMS materials, the protein was in a significantly higher abundance on PDMS-9kPa (MFC of 15). On the HA materials, the difference in FimA abundance cannot be considered as significant as p-value > 0.05. It should be noted that FimH was not identified on a material. This was expected as FimH is the subunit located at the Type-1 pili tip. It could thus only be identified in the secretome [1]. [1] Hwang, S.; Öster, C.; Chevelkov, V.; Giller, K.; Lange, S.; Becker, S.; Lange, A., Characterization of H/D exchange in type 1 pili by proton-detected solid-state NMR and molecular dynamics simulations. J. Biomol. NMR 2019, 73 (6), 281-291, 10.1007/s10858-019-00247-.

A

Name	Short name	MFC	
		PDMS	HA
NADH:ubiquinone oxidoreductase, chain G	nuoG	1.8	1.6
pyruvate dehydrogenase, decarboxylase component E1, thiamin-binding	aceE	2.4	1.7
fused acetaldehyde-CoA dehydrogenase/iron-dependent alcohol dehydrogenase/pyruvate-formate lyase deactivase	adhE	4.0	2.6
phenylalanine tRNA synthetase, beta subunit	pheT	1.6	1.6

B

Material	*p*-value (ANOVA)	MFC	Mean abundance
HA	$8.92\ 10^{-2}$	1.9	$1.5\ 10^{5}$ (HA-2kPa)
PDMS	$2.08\ 10^{-3}$	15.0	$1.6\ 10^{6}$ (PDMS-9kPa)

In summary, the bacterial mechanical environment significantly regulates MscS mechanosensitive channel (higher abundance on the least colonized HA-44Pa) and Type-1 pili [71] (higher abundance on the most colonized PDMS-9kPa). Busscher and coworkers recently demonstrated that the contact of *Staphylococcus aureus* with a surface creates adhesion force triggering the mechanosensitive channel MscL [61]. Here, the mechanosensitive channel MscS is probably triggered in *E. coli* by a similar mechanism. Because of the low critical force necessary to open these channels, it may even allow the bacterium to distinguish between elasticity favorable or detrimental to the survival on the surface. Furthermore, Type-1 pili allow bacteria to attach to surfaces in a force-dependent, so-called "catch-bond", manner, due to changes in pili structure (coiling, uncoiling) [76,77]. This ability of Type-1 pili to retract under external forces makes them possible sensors of the surface elasticity as well as adaptive tethers. The structure and quantity of Type-1 pili may change depending on the surface stiffness for a given condition of shear stress. A similar process may occur when an adherent bacterium is exposed to an increase and decrease in shear stress for a given surface stiffness.

Finally, the difference in the protein patterns confirms that tethers (Type-1 pili) are rare or almost absent on the hydrated HA surfaces, whereas they are far more abundant on the PDMS surfaces. This is consistent with the expected role of Type-1 pili as tether, favorable to bacterial adhesion. On PDMS-9kPa in particular, the high abundance of Type-1 pili is expected to strengthen the link between bacteria and the surface, and thus to enhance bacterial stability and further bacterial growth on the surface.

3.3. Bacteria are confined to all surfaces except PDMS-9kPa, and are less diffusive on soft surfaces

Next, given that tethers are thought to hinder mobility, we investigated whether mechanical conditions govern adherent bacteria's ability to move about, which is critical for bacterial colonization. Since proteins associated with *E. coli* motility were not in significant abundance in the protein patterns, we presumed that mobility was merely a consequence of Brownian motion. The fraction of mobile *E. coli* cells in the total sessile population, defined as cells that moved at least 2 μm from their initial position (d_{net} at the maximal observation time, Figure

2), varied with the material (Figure 6). It was similar on HA-2kPa, PDMS-9kPa and PDMS-574kPa, but was about 3 times lower on HA-44Pa. Along with the low quantity of sessile bacteria, most of the "immobile" bacteria observed on HA-44kPa probably revealed their difficulty in maintaining contact with this surface. Only bacteria anchored to the surface probably remained sessile. In contrast, slightly adhered bacteria, such as those moving on a surface, were easily removed by any slight movement of the liquid due to the temperature or the washing process. On the contrary, moving bacteria adhered tightly enough to the other types of materials (HA-2kPa, PDMS-9kPa and PDMS-574kPa) to maintain contact with the surface. In addition, indentation of the material by sessile bacteria is expected to be more than 10 times higher on a surface with Young's modulus of 44 Pa (1.8 nm) than on surfaces with Young's moduli above 2 kPa, (0.13 nm for 2 kPa) (Figure S8). This may have favored frictional forces during mobility and the subsequent reduction in bacterial movements. Finally, as mobility of bacterial cells on surfaces is thought to facilitate expansion of the sessile population, this may have restricted colonization of the HA-44Pa in comparison to what occurred on the other surfaces. This is in agreement with the low colonization observed at short- and longer-term on this surface.

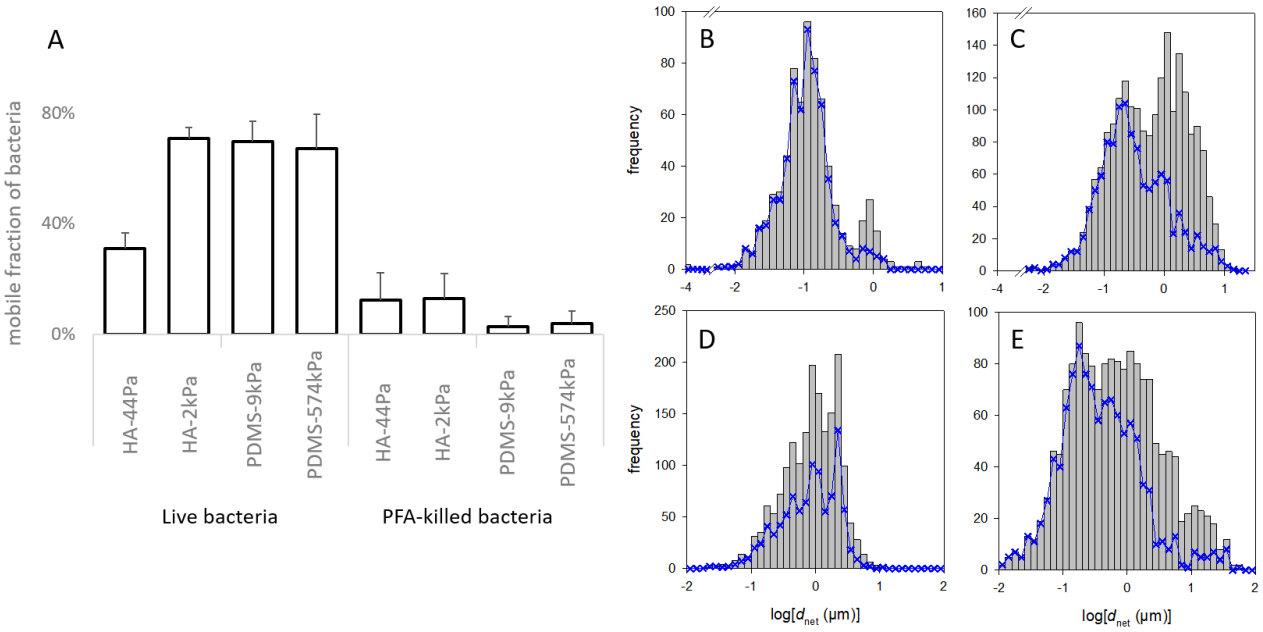

Figure 6. Mobility of bacterial cells on HA and PDMS materials: (A) Fraction of live and killed bacteria with displacement of more than 2 µm in the entire observation period ("mobile fraction"); (B-E) Frequency of dnet of bacteria on HA-44Pa (B), HA-2kPa (C), PDMS-9kPa (D) and PDMS-574kPa (E) materials. The grey histograms encompass all tracks recorded over the entire observation time (i.e. about 1 min) at the successive times where pictures were taken (e.g. 3, 6, …, 57 s). The blue curves correspond only to those tracks that could be followed over the whole observation time (e.g. 57 s).

It is important to note that mobility of bacterial cells previously killed with PFA solution, thus considered as inert objects, (Figure 6A) was much less than mobility of live cells whatever the material (from 62% to 98% less). This suggests that characteristics of the live cells were crucial for a large part of the observed mobility. These characteristics may have been purely biological, allowing for example active mobility or active anchorage on the surface, or have been related to the physicochemical properties of the bacterial surface and appendages. However, they could have been modified by the PFA treatment.

Furthermore, motion of live bacteria significantly differed between cells on the same material surface, as shown by the frequency of d_{net} on each material type (typical examples in Figure 6B-E). More specifically, the non-linearity of logΦ with respect to d_{net}^2 (measured at a given time on a given sample) suggests that several

subpopulations of bacteria made up the whole population (example of Φ function of a PDMS-574kPa sample in Figure 7A) (please refer to the Experimental section part "Data and statistical analysis" for more details). Such coexistence of bacterial subpopulations differing in mobility is not surprising and is known in planktonic and sessile populations [78,79]. However, only Song *et al*. reported that such a heterogeneity may vary with surface stiffness [80]. In addition, the relation of $< d_{net}^2 >$ to t suggested that, on some surfaces, bacteria were confined to one area rather than diffusing freely. Indeed, this relation was linear within the statistical fluctuations on several surfaces as expected for a free Brownian motion, but also showed a strong deviation from this law for other surfaces (examples in Figure S9). This limitation in the cell movement may correspond to their attachment to the surface through an elastic bond.

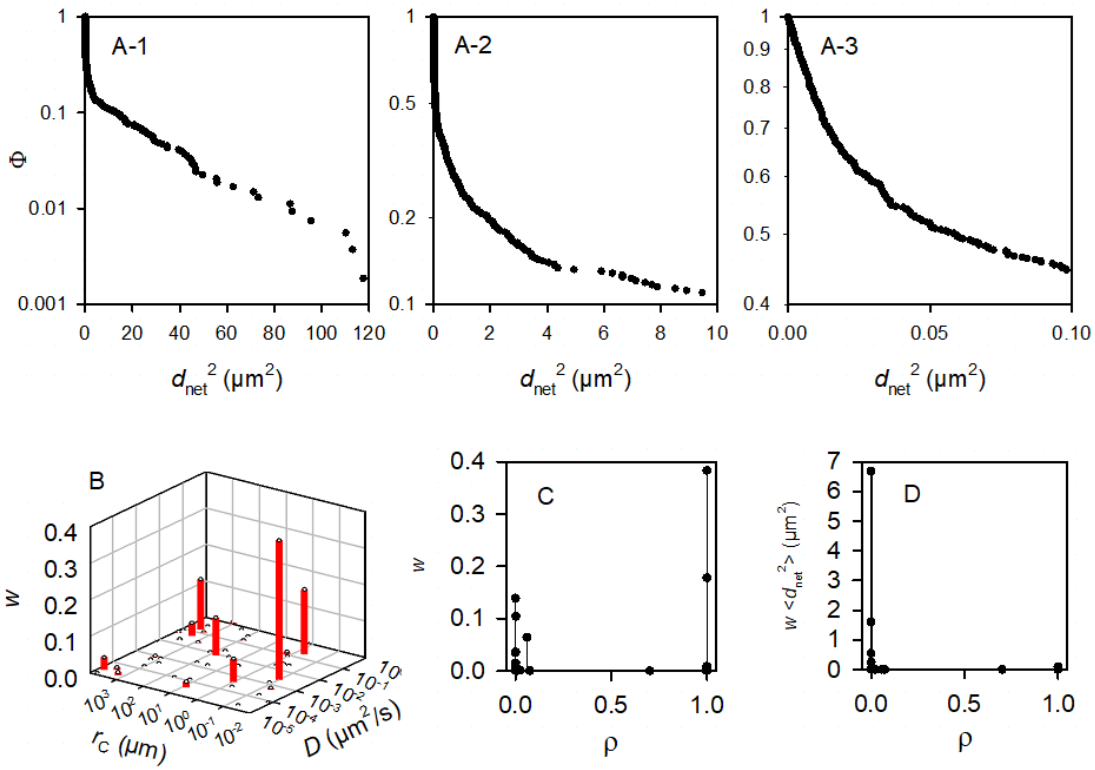

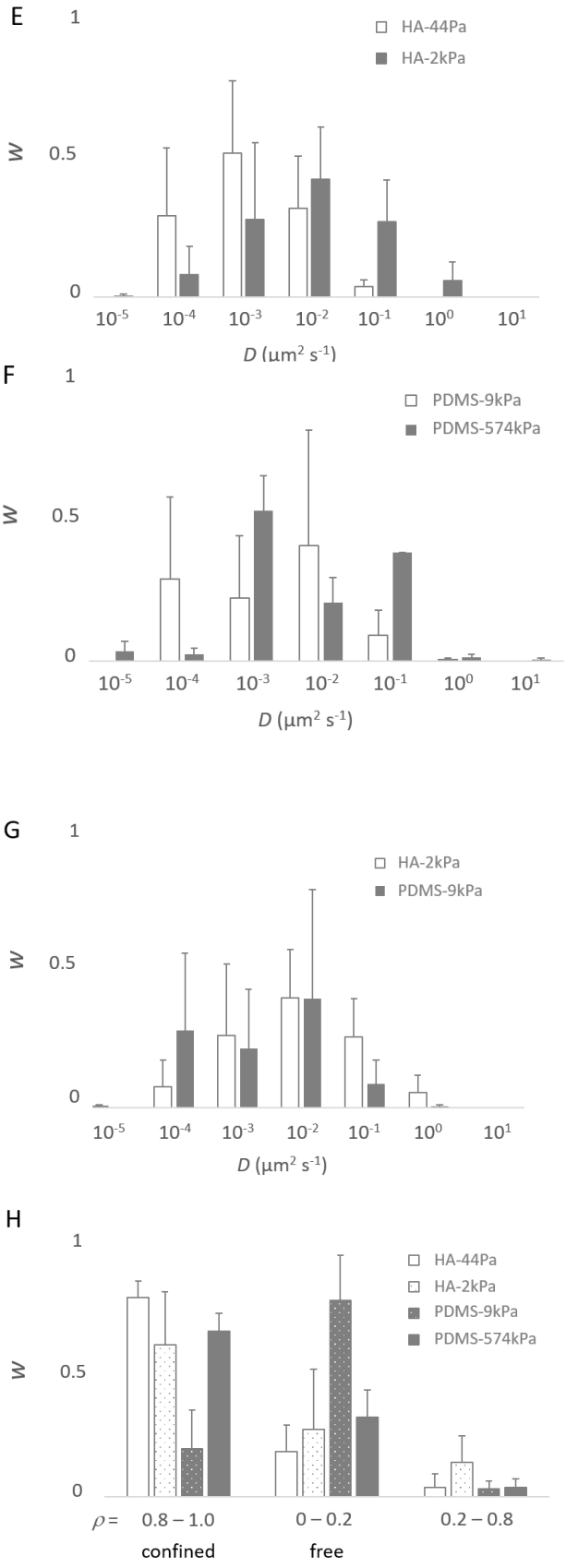

Figure 7. Modeling of the movement of bacteria. From (A) to (D), the bacteria were deposited on a PDMS-574kPa sample and the model accounted for $m = 50$ subpopulations. As made visible by (B), less than $m = 10$ subpopulations are sufficient

to describe the population. Panels (E) to (H) were accordingly based on computations with m = 10. (A) Experimental complementary cumulative frequency Φ of $<d_{net}^2>$ at various scales (A-1, A-2, A3) of the x axis for the purpose of showing that Φ is not a single exponentially decreasing function; (B) Relative weight, w, of the subpopulations characterized by their specific D and r_C parameters; (C) Relative importance of the free (ρ ~ 0) and confined (ρ ~ 1) bacterial subpopulations; (D) Contribution of the subpopulations characterized by a confinement index ρ to the mean square displacement or $<d_{net}^2>$; (E-G). Relative fractions, w, of the main bacterial subpopulations ($\sum w_i$ > 99 %), in the whole population, as a function of the diffusion coefficient, D (D are grouped into [0.5 10^{-z} , 5.0 10^{-z}[classes with z ∈ {-1, 0, 1, 2, 3, 4, 5}): comparison between HA-44Pa and HA-2kPa materials (E), between PDMS-9kPa and PDMS-574kPa materials (F) and between HA-2kPa and PDMS-9kPa materials (G); (H) Fractions, w, of the main bacterial subpopulations as a function of the confinement index, ρ.

To identify whether the sessile population might vary in these terms depending on the surface nature and surface stiffness, we modeled the Φ functions with m subpopulations of bacterial cells with homogeneous motion characteristics, and we considered the bacterial cells as Brownian particles moving in harmonic energy wells (Equation 2). It is worth noting that the aim here was to dissect the observation rather than to propose a final, explanatory model. Therefore, we chose to consider Brownian motion with different levels of confinement depending on the parameter r_C, for the sake of simplicity, but it is possible that in reality, confined and sub-diffusion Brownian motions may combine [32]. Starting from the hypothesis that the population encompasses several subgroups, modeling of the 19 experimental Φ functions of a PDMS-574kPa sample (after times 3, 6, …, 57 s) with m = 50 subpopulations confirmed that the total population was accounted for. Each of these m subpopulations was defined by D, the diffusion coefficient, r_C, the radius and w, the relative fraction in the whole population (Figure 7B), as well as by the confinement index ρ as the quantification of the level of freedom of bacteria within a subpopulation (Equation 7 and Figure 7C,D). By convention, bacteria were considered free for $\rho \leq 0.2$ and confined for $\rho \geq 0.8$. This example shows that fewer than 10 subpopulations gather more than 99 % of the tracks (Figure 7B). This suggested that we restrict the number of subpopulations to m = 10 for further modeling. Typical results of the modeling with m = 10 that best fit the experimental Φ functions of $<d_{net}^2>$ measured on a sample are shown in Table S3 for each material type. The results confirm that tracks (each corresponding to one bacterium) can be grouped into few subpopulations (from 3 to 8 depending on the sample). Only rare bacteria (less than 1 % of the total tracked population) were identified with other motion characteristics.

In general, the results show that the diffusion of cells globally increased with the surface stiffness. In other words, subpopulations with higher diffusion coefficients were more frequent or contained more cells on materials with higher stiffness (Figure 7E-G), whereas, on the contrary, subpopulations with low diffusion coefficients were more frequent when the surface stiffness decreased. In that respect, subpopulations on the PDMS-574kPa surface revealed diffusion coefficients higher than those of subpopulations identified on the PDMS-9kPa (Figure 7F), and the diffusion coefficients on surfaces of similar elasticity (HA-2kPa and PDMS-9kPa) were distributed similarly (Figure 7G). In addition, the bacterial population on the HA-44Pa surface was composed of subpopulations with diffusion coefficients usually smaller (maximum at 10^{-3} μm^2 s^{-1}) than those of subpopulations on the HA-2kPa surface (maximum at 10^{-2} μm^2 s^{-1}) (Figure 7E). Furthermore, the confinement of cells did not globally increase or decrease with the surface stiffness. Rather, the fraction of free bacteria (i.e., with ρ from 0 to 0.2) increased with bacterial adhesion, however without significant correlation (R^2 = 0.78; Figure 8). Typically, bacterial subpopulations were the most confined on HA-44Pa, the least colonized surface. They were less confined on the HA-2kPa and PDMS-574kPa materials (Figure 7H) and revealed a predominant un-confined motion on PDMS-9kPa.

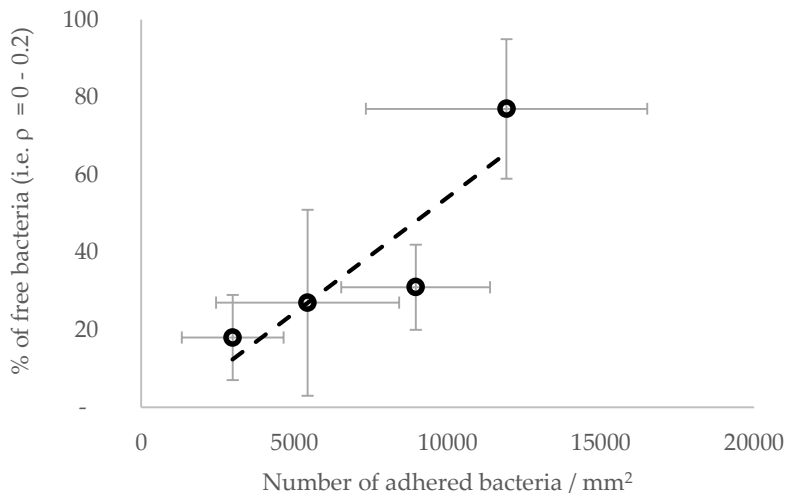

Figure 8. Fraction of free bacteria (i.e., with ρ from 0 to 0.2) depending on the resulting, further bacterial adhesion. The most significant linear correlation is given by the broken line ($R^2 = 0.78$).

Overall, these results indicate that diffusion and confinement are not correlated, but that diffusion correlates with surface stiffness, whereas confinement oppositely correlates with adhesion rate. Typically, bacteria tend to move very little on HA-44Pa, slightly more on HA-2kPa and much more on PDMS-574kPa, but stay at a nearly constant location on the three surfaces. On the PDMS-9kPa surface, bacteria tend to move as little as on HA-2kPa but much farther away from their initial location (Figure 5B). This displacement, characterized as to be free on the basis of our model, is associated with more bacterial adhesion, more biofilm formation, and significantly higher abundance of Type-1 pili compared to the other surfaces (Figure 5A). This suggests that free motion is crucial for allowing bacteria to colonize a surface. These observations are consistent with the significant contribution to population expansion attributed to bacterial mobility by other authors[81]. However, free displacement may be in contradiction with the higher abundance of Type-1 pili on the PDMS-9kPa surface. Indeed, pili are thought to be responsible for tethering of bacterial cells to a surface and for stable bacterial adhesion [82].

Nevertheless, pili may also be favorable to bacterial mobility on surfaces, as suggested by the works of Busscher's and Vogel's groups [60,83,84]. In that respect, Sjollema *et al.* demonstrated that successive detachment and attachment of multiple tethers between bacteria and the surface, such as those created by pili, can lead to sub-micrometric displacements under thermal agitation [60,83,84]. Thomas *et al*. also reported the combination of rolling motion and pili attachment of *E. coli* cells on a surface under various flow rates [84]. Such way of motion may be a sub-class of the gliding motion class with pili (also known as twitching) [85], which concerns individual, sparse, and sessile bacterial cells, and is favored on soft surfaces [86] in a range of speed (0.06 –1.4 μm s^{-1}) consistent with the bacterial speeds estimated from the modeled results reported here (0.01-4 μm s^{-1}; for calculation, see Equation 7). Twitching is usually mediated by Type-IV pili [87], which *E. coli* K12 lacks under laboratory conditions, despite the presence of the appropriate genes [88], but, as noted by Harshey *et al*. [89], several different mechanisms may compose gliding as a whole. Some of them are probably still unknown.

Pili-related motion through attachment/detachment cycles was reported as not being free by Sjollema *et al.* [83]. However, this may depend on surface properties, as tether strengths and detachment/attachment dynamics should depend on them. In particular, surface stiffness may be more or less favorable to detachment/attachment cycles depending on the deformation of the surface allowed at the pili-tethering locations when the attached bacterium is rolling (Figure 5C). Our hypothesis is that a softer surface reduces

the traction force applied on the pili during rolling compared to what happens on a stiffer surface. This may prevent the pili from strengthening the link to the surface as expected with a catch-bond submitted to increasing forces, or the tether to detach if the force becomes higher than the force threshold needed to break the catch-bond. In such a scenario, an optimal stiffness should exist depending on the rupture force of the catch-bond, which should allow the bacterium to freely move while staying attached to the surface thanks to pili-tethers. Such motion should require the replacement and, thus, more pili production than when the bacterium stays attached to a constant location. Therefore, with this hypothesis, the optimal stiffness allowing such mobility on PDMS is here estimated to be close to a few kPa or a few tens kPa, as PDMS-9kPa is more favorable to free motion and higher pili abundance than PDMS-574kPa. On HA-44Pa and HA-2kPa surfaces, such motion may be hindered by the hydration layer that prevents the attachment of pili to the surface. On these surfaces as well as on PDMS-574kPa, bacterial motion may only be governed by agitation in the medium combined with friction forces between bacterium wall and the surface. These forces should depend on the bacterium-to-surface indentation, directly correlated to the surface stiffness, and thus be responsible for the increase in diffusion coefficient observed when the stiffness increases, and for the higher confinement observed on the very soft HA-44Pa.

4. Conclusions

Our results confirm that elasticity is a surface property that can be optimized to regulate the formation of biofilms on materials. However, this benefit is counterbalanced by a high degree of surface hydration. We have established that increasing softness is an efficient way of disturbing bacterial mobility and inhibiting biofilm formation on HA-based materials. Importantly, free-moving bacterial subpopulations were the rarest on the softest HA (HA-44Pa), which revealed the most confined and least diffusive subpopulations, and was the least colonized material. In contrast, biofilm formation progress was ahead of time on the non-hydrated PDMS (PDMS-9kPa) compared to the hydrated HA material with similar stiffness (HA-2kPa). In line with this, a protein of Type-1 pili, that tethers bacteria to surfaces, was detected in large quantities on the PDMS-9kPa surface, while several overproduced proteins conform to an early phase of bacterial adhesion. The mobility of sessile bacteria also varied from one surface to another: In general, their diffusion coefficients increased when elasticity increased, while their confinement oppositely correlated with biofilm formation. This shows that freedom of mobility, but not diffusion, is favorable to biofilm formation, and suggests that it could be a predictive indicator for biofilm formation. The overall findings also suggest that the mobility observed on the most colonized, PDMS-9kPa, material is related to the use by bacteria of Type-1 pili through a turn-over of their attachment and detachment from the material surface. Finally, this study gives important insights into how to improve the elasticity and hydration of biomaterials made of PDMS, HA and other hydrogel materials to hinder their infection by bacteria.

Supplementary Materials: The following supporting information can be downloaded at: www.mdpi.com/xxx/s1, Figure S1: title; Table S1: title; Video S1: title.

Author Contributions: Annabelle Vigué: investigation & formal analysis (microbiology, microscopy, material production and characterization), methodology, visualization, writing – original draft Dominique Vautier: conceptualization, project administration, supervision, writing – review; Amad Kaytoue: investigation (microbiology, microscopy) ; Bernard Senger: formal analysis (computer simulation and modeling), writing – review; Youri Arntz: investigation (AFM); Vincent Ball: investigation & formal analysis (rheology), writing – review; Amine Ben Mlouka: investigation & formal analysis (proteomic analysis); Varvara Gribova: conceptualization (HA hydrogels), writing – review; Samar Hajjar-Garreau: investigation & formal analysis (XPS), writing – review; Julie Hardouin: formal analysis (proteomic analysis), writing – review; Thierry Jouenne: conceptualization, formal analysis (proteomic analysis), writing – review; Philippe Lavalle:

funding acquisition, writing – review; Lydie Ploux: conceptualization, project administration, resources, supervision, validation, methodology, formal analysis (microbiology, microscopy, proteomic analysis, material characterization), visualization, writing – original draft, review & editing

Data Availability Statement: The mass spectrometry proteomics data have been deposited to the ProteomeXchange Consortium via the PRIDE [90] partner repository with the dataset identifier PXD035233.

Acknowledgments: The authors would like to thank the Region Grand Est (ERMES project), the ANR (BABE project) as well as the "Groupement de Recherche" GDR B2I (GDR3751) for their supports. They would also like to thank Prof. Corinne Nardin and Victor Igbokwe for their considerable help in reviewing the manuscript.

Conflicts of Interest: The authors declare no conflict of interest.

References

1. Spellberg, B.; Guidos, R.; Gilbert, D.; Bradley, J.; Boucher, H.W.; Scheld, W.M.; Bartlett, J.G.; Edwards, J., Jr. The epidemic of antibiotic-resistant infections: a call to action for the medical community from the Infectious Diseases Society of America. *Clin. Infect. Dis.* **2008**, *46*, 155-164, doi:10.1086/524891.

2. World Health, O. *Antibiotic resistance: multi-country public awareness survey*; World Health Organization: Geneva, 2015.

3. Costerton, J.W.; Stewart, P.S.; Greenberg, E.P. Bacterial biofilms : a common cause of persistent infections. *Science* **1999**, *284*, 1318-1322.

4. Beloin, C.; Roux, A.; Ghigo, J.M. Escherichia coli biofilms. In *Bacterial Biofilms*, Romeo, T., Ed.; Springer Berlin Heidelberg: Berlin, Heidelberg, 2008; pp. 249-289.

5. Bakker, D.P.; Huijs, F.M.; de Vries, J.; Klijnstra, J.W.; Busscher, H.J.; van der Mei, H.C. Bacterial deposition to fluoridated and non-fluoridated polyurethane coatings with different elastic modulus and surface tension in a parallel plate and a stagnation point flow chamber. *Colloids and Surfaces B: Biointerfaces* **2003**, *32*, 179-190, doi:10.1016/S0927-7765(03)00159-0.

6. Cottenye, N.; Anselme, K.; Ploux, L.; Vebert-Nardin, C. Vesicular structures self-assembled from oligonucleotide-polymer hybrids: Mechanical prevention of bacterial colonization upon their surface tethering through hybridization. *Adv. Funct. Mater.* **2012**, *5*, 4891–4898, doi:10.1002/adfm.201200988.

7. Lichter, J.A.; Thompson, M.T.; Delgadillo, M.; Nishikawa, T.; Rubner, M.F.; Van Vliet, K.J. Substrata mechanical stiffness can regulate adhesion of viable bacteria. *Biomacromolecules* **2008**, *9*, 1571-1578, doi:10.1021/bm701430y.

8. Saha, N.; Monge, C.; Dulong, V.; Picart, C.; Glinel, K. Influence of polyelectrolyte film stiffness on bacterial growth. *Biomacromol.* **2013**, *14*, 520-528, doi:10.1021/bm301774a.

9. Harapanahalli, A.K.; Younes, J.A.; Allan, E.; van der Mei, H.C.; Busscher, H.J. Chemical signals and mechanosensing in bacterial responses to their environment. *PLoS Pathog.* **2015**, *11*, e1005057, doi:10.1371/journal.ppat.1005057.

10. Dufrêne, Y.F.; Persat, A. Mechanomicrobiology: how bacteria sense and respond to forces. *Nat. Rev. Microbiol.* **2020**, *18*, 227-240, doi:10.1038/s41579-019-0314-2.

11. Liu, X.; Zhu, K.; Duan, X.; Wang, P.; Han, Y.; Peng, W.; Huang, J. Extracellular matrix stiffness modulates host-bacteria interactions and antibiotic therapy of bacterial internalization. *Biomaterials* **2021**, *277*, 121098, doi:10.1016/j.biomaterials.2021.121098.

12. Song, F.; Ren, D. Stiffness of cross-linked poly(dimethylsiloxane) affects bacterial adhesion and antibiotic susceptibility of attached cells. *Langmuir* **2014**, *30*, 10354-10362, doi:10.1021/la502029f.

13. Straub, H.; Bigger, C.M.; Valentin, J.; Abt, D.; Qin, X.-H.; Eberl, L.; Maniura-Weber, K.; Ren, Q. Bacterial adhesion on soft materials: passive physicochemical interactions or active bacterial mechanosensing? *Advanced Healthcare Materials* **2019**, *8*, 1801323, doi:10.1002/adhm.201801323.

14. Guégan, C.; Garderes, J.; Le Pennec, G.; Gaillard, F.; Fay, F.; Linossier, I.; Herry, J.M.; Fontaine, M.N.B.; Réhel, K.V. Alteration of bacterial adhesion induced by the substrate stiffness. *Colloids and Surfaces B: Biointerfaces* **2014**, *114*, 193-200, doi:10.1016/j.colsurfb.2013.10.010.

15. Kolewe, K.W.; Peyton, S.R.; Schiffman, J.D. Fewer bacteria adhere to softer hydrogels. *ACS Appl. Mater. Interfaces* **2015**, *7*, 19562-19569, doi:10.1021/acsami.5b04269.

16. Highley, C.B.; Prestwich, G.D.; Burdick, J.A. Recent advances in hyaluronic acid hydrogels for biomedical applications. *Curr. Opin. Biotechnol.* **2016**, *40*, 35-40, doi:10.1016/j.copbio.2016.02.008.

17. Schuurmans, C.C.L.; Mihajlovic, M.; Hiemstra, C.; Ito, K.; Hennink, W.E.; Vermonden, T. Hyaluronic acid and chondroitin sulfate (meth)acrylate-based hydrogels for tissue engineering: Synthesis, characteristics and pre-clinical evaluation. *Biomaterials* **2021**, *268*, 120602, doi:10.1016/j.biomaterials.2020.120602.

18. Gribova, V.; Boulmedais, F.; Dupret-Bories, A.; Calligaro, C.; Senger, B.; Vrana, N.E.; Lavalle, P. Polyanionic hydrogels as reservoirs for polycationic antibiotic substitutes providing prolonged antibacterial activity. *ACS Appl. Mater. Interfaces* **2020**, *12*, 19258-19267, doi:10.1021/acsami.9b23140.

19. Shirley, D.A. High-resolution X-ray photoemission spectrum of the valence bands of gold. *Physical Review B* **1972**, *5*, 4709-4714, doi:10.1103/PhysRevB.5.4709.

20. Beamson, G.; Briggs, D. High resolution XPS of organic polymers: the Scienta ESCA300 database. *J. Chem. Educ.* **1993**, *70*, A25, doi:10.1021/ed070pA25.5.

21. Alexander , M.R.; Short , R.D.; Jones , F.R.; Michaeli , W.; Blomfield, C.J. A study of HMDSO/O2 plasma deposits using a high-sensitivity and -energy resolution XPS instrument: curve fitting of the Si 2p core level. *Appl. Surf. Sci.* **1999**, *137*, 179–183.

22. Nečas, D.; Klapetek, P. Gwyddion: an open-source software for SPM data analysis. *Open Physics* **2012**, *10*, 181-188, doi:doi:10.2478/s11534-011-0096-2.

23. Carrier, O.; Bonn, D. Chapter 2 - Contact angles and the surface free energy of solids. In *Droplet Wetting and Evaporation*, Brutin, D., Ed.; Academic Press: Oxford, 2015; pp. 15-23.

24. Law, K.-Y. Definitions for hydrophilicity, hydrophobicity, and superhydrophobicity: getting the basics right. *The Journal of Physical Chemistry Letters* **2014**, *5*, 686-688, doi:10.1021/jz402762h.

25. Vidal, O.; Longin, R.; Prigent-Combaret, C.; Dorel, C.; Hooreman, M.; Lejeune, P. Isolation of an Escherichia coli K-12 mutant strain able to form biofilms on inert surfaces: involvement of a new ompR allele that increases curli expression. *J. Bacteriol.* **1998**, *180*, 2442-2449.

26. Antonovaite, N.; Beekmans, S.V.; Hol, E.M.; Wadman, W.J.; Iannuzzi, D. Regional variations in stiffness in live mouse brain tissue determined by depth-controlled indentation mapping. *Scientific Reports* **2018**, *8*, 12517, doi:10.1038/s41598-018-31035-y.

27. Dimitriadis, E.K.; Horkay, F.; Maresca, J.; Kachar, B.; Chadwick, R.S. Determination of elastic moduli of thin layers of soft material using the atomic force microscope. *Biophys. J.* **2002**, *82*, 2798-2810, doi:10.1016/S0006-3495(02)75620-8.

28. Miao, H.; Ratnasingam, S.; Pu, C.S.; Desai, M.M.; Sze, C.C. Dual fluorescence system for flow cytometric analysis of Escherichia coli transcriptional response in multi-species context. *J. Microbiol. Methods* **2009**, *76*, 109-119, doi:10.1016/j.mimet.2008.09.015.

29. de Gennes, P.G. Wetting: statics and dynamics. *Reviews of Modern Physics* **1985**, *57*, 827-863, doi:10.1103/RevModPhys.57.827.

30. Rasband, W., U. S. National Institutes of Health, Bethesda, Maryland, USA *ImageJ*, 1997.

31. Heydorn, A.; Nielsen, A.T.; Hentzer, M.; Sternberg, C.; Givskov, M.; Ersboll, B.K. Quantification of biofilm structures by the novel computer program COMSTAT. *Microbiology (Moscow, Russ. Fed.)* **2000**, *146*, 2395–2407, doi:10.1099/00221287-146-10-2395.

32. Meijering, E.; Dzyubachyk, O.; Smal, I. Methods for cell and particle tracking. *Methods Enzymol.* **2012**, *504*, 183-200, doi:10.1016/b978-0-12-391857-4.00009-4.

33. Kirkpatrick, S.; Gelatt, C.D.; Vecchi, M.P. Optimization by simulated annealing. *Science* **1983**, *220*, 671-680, doi:10.1126/science.220.4598.671.

34. Kentache, T.; Ben Abdelkrim, A.; Jouenne, T.; Dé, E.; Hardouin, J. Global dynamic proteome study of a pellicle-forming Acinetobacter baumannii strain. *Mol. Cell. Proteomics* **2017**, *16*, 100-112, doi:10.1074/mcp.M116.061044.

35. Obry, A.; Hardouin, J.; Lequerré, T.; Jarnier, F.; Boyer, O.; Fardellone, P.; Philippe, P.; Marcelli, C.; Loët, X.L.; Vittecoq, O.; et al. Identification of 7 proteins in sera of RA patients with potential to predict ETA/MTX treatment response. *Theranostics* **2015**, *5*, 1214-1224, doi:10.7150/thno.12403.

36. Ladam, G.; Vonna, L.; Sackmann, E. Micromechanics of surface-grafted hyaluronic acid gels. *The Journal of Physical Chemistry B* **2003**, *107*, 8965-8971, doi:10.1021/jp0272872.

37. Valentin, J.D.P.; Qin, X.-H.; Fessele, C.; Straub, H.; van der Mei, H.C.; Buhmann, M.T.; Maniura-Weber, K.; Ren, Q. Substrate viscosity plays an important role in bacterial adhesion under fluid flow. *J. Colloid Interface Sci.* **2019**, *552*, 247-257, doi:10.1016/j.jcis.2019.05.043.

38. Drebezghova, V.; Hakil, F.; Grimaud, R.; Gojzewski, H.; Vancso, G.J.; Nardin, C. Initial bacterial retention on polydimethylsiloxane of various stiffnesses: The relevance of modulus (mis)match. *Colloids and Surfaces B: Biointerfaces* **2022**, *217*, 112709, doi:10.1016/j.colsurfb.2022.112709.

39. Mata, A.; Fleischman, A.J.; Roy, S. Characterization of polydimethylsiloxane (PDMS) properties for biomedical micro/nanosystems. *Biomedical microdevices* **2005**, *7*, 281-293, doi:10.1007/s10544-005-6070-2.

40. Qin, X.-H.; Senturk, B.; Valentin, J.; Malheiro, V.; Fortunato, G.; Ren, Q.; Rottmar, M.; Maniura-Weber, K. Cell-membrane-inspired silicone interfaces that mitigate proinflammatory macrophage activation and bacterial adhesion. *Langmuir* **2019**, *35*, 1882-1894, doi:10.1021/acs.langmuir.8b02292.

41. Hermansson, M. The DLVO theory in microbial adhesion. *Colloids and Surfaces B: Biointerfaces* **1999**, *14*, 105-119.

42. Poortinga, A.T.; Bos, R.; Norde, W.; Busscher, H.J. Electric double layer interactions in bacterial adhesion to surfaces. *Surf. Sci. Rep.* **2002**, *47*, 1-32.

43. Bos, R.; van der Mei, H.C.; Gold, J.; Busscher, H.J. Retention of bacteria on a substratum surface with micro-patterned hydrophobicity. *FEMS Microbiol. Lett.* **2000**, *189*, 311-315.

44. Chhasatia, V.H.; Sun, Y. Interaction of bi-dispersed particles with contact line in an evaporating colloidal drop. *Soft Matter* **2011**, *7*, 10135-10143, doi:10.1039/C1SM06393F.

45. Anselme, K.; Davidson, P.; Popa, A.M.; Giazzon, M.; Liley, M.; Ploux, L. Response to comment on "The interaction of cells and bacteria with surfaces structures at the nanoscale". *Acta Biomater.* **2011**, *7*, 1936-1937, doi:DOI: 10.1016/j.actbio.2010.12.002.

46. Pan, F.; Altenried, S.; Liu, M.; Hegemann, D.; Bülbül, E.; Moeller, J.; Schmahl, W.W.; Maniura-Weber, K.; Ren, Q. A nanolayer coating on polydimethylsiloxane surfaces enables a mechanistic study of bacterial adhesion influenced by material surface physicochemistry. *Materials Horizons* **2020**, *7*, 93-103, doi:10.1039/C9MH01191A.

47. Siddiqui, S.; Chandrasekaran, A.; Lin, N.; Tufenkji, N.; Moraes, C. Microfluidic shear assay to distinguish between bacterial adhesion and attachment strength on stiffness-tunable silicone substrates. *Langmuir* **2019**, *35*, 8840-8849, doi:10.1021/acs.langmuir.9b00803.

48. Peng, Q.; Zhou, X.; Wang, Z.; Xie, Q.; Ma, C.; Zhang, G.; Gong, X. Three-dimensional bacterial motions near a surface investigated by digital holographic microscopy: effect of surface stiffness. *Langmuir* **2019**, *35*, 12257-12263, doi:10.1021/acs.langmuir.9b02103.

49. Kolewe, K.W.; Kalasin, S.; Shave, M.; Schiffman, J.D.; Santore, M.M. Mechanical properties and concentrations of poly(ethylene glycol) in hydrogels and brushes direct the surface transport of Staphylococcus aureus. *ACS Appl. Mater. Interfaces* **2019**, *11*, 320-330, doi:10.1021/acsami.8b18302.

50. Wang, Y.; Guan, A.; Isayeva, I.; Vorvolakos, K.; Das, S.; Li, Z.; Phillips, K.S. Interactions of Staphylococcus aureus with ultrasoft hydrogel biomaterials. *Biomaterials* **2016**, *95*, 74-85, doi:10.1016/j.biomaterials.2016.04.005.

51. Keskin, D.; Mergel, O.; van der Mei, H.C.; Busscher, H.J.; van Rijn, P. Inhibiting bacterial adhesion by mechanically modulated microgel coatings. *Biomacromolecules* **2019**, *20*, 243-253, doi:10.1021/acs.biomac.8b01378.

52. Lee, S.W.; Phillips, K.S.; Gu, H.; Kazemzadeh-Narbat, M.; Ren, D. How microbes read the map: Effects of implant topography on bacterial adhesion and biofilm formation. *Biomaterials* **2021**, *268*, 120595, doi:10.1016/j.biomaterials.2020.120595.

53. Ploux, L.; Ponche, A.; Anselme, K. Bacteria/material interfaces: role of the material and cell wall properties. *J. Adhes. Sci. Technol.* **2010**, *24*, 2165-2201.

54. Busscher, H.J.; Norde, W.; van der Mei, H.C. Specific molecular recognition and nonspecific contributions to bacterial interaction forces. *Appl. Environ. Microbiol.* **2008**, *74*, 2559-2564, doi:10.1128/aem.02839-07.

55. Del Grosso, C.A.; Leng, C.; Zhang, K.; Hung, H.-C.; Jiang, S.; Chen, Z.; Wilker, J.J. Surface hydration for antifouling and bio-adhesion. *Chemical Science* **2020**, *11*, 10367-10377, doi:10.1039/D0SC03690K.

56. Chen, S.; Li, L.; Zhao, C.; Zheng, J. Surface hydration: principles and applications toward low-fouling/nonfouling biomaterials. *Polymer* **2010**, *51*, 5283-5293, doi:10.1016/j.polymer.2010.08.022.

57. Ong, Y.L.; Razatos, A.; Georgiou, G.; Sharma, M.M. Adhesion forces between E.coli bacteria and biomaterial surfaces. *Langmuir* **1999**, *15*, 2719-2725.

58. Böhmler, J.; Haidara, H.; Ponche, A.; Ploux, L. Impact of chemical heterogeneities of surfaces on colonization by bacteria. *ACS Biomaterials Science & Engineering* **2015**, *2015*, 693–704, doi:10.1021/acsbiomaterials.5b00151.

59. Busscher, H.J.; van der Mei, H.C. How do bacteria know they are on a surface and regulate their response to an adhering state? *PLoS Pathog.* **2012**, *8*, e1002440, doi:10.1371/journal.ppat.1002440.

60. Carniello, V.; Peterson, B.W.; van der Mei, H.C.; Busscher, H.J. Physico-chemistry from initial bacterial adhesion to surface-programmed biofilm growth. *Adv. Colloid Interface Sci.* **2018**, *261*, 1-14, doi:10.1016/j.cis.2018.10.005.

61. Carniello, V.; Peterson, B.W.; van der Mei, H.C.; Busscher, H.J. Role of adhesion forces in mechanosensitive channel gating in Staphylococcus aureus adhering to surfaces. *NPJ Biofilms Microbiomes* **2020**, *6*, 31, doi:10.1038/s41522-020-00141-z.

62. van den Berg, J.; Galbiati, H.; Rasmussen, A.; Miller, S.; Poolman, B. On the mobility, membrane location and functionality of mechanosensitive channels in Escherichia coli. *Scientific Reports* **2016**, *6*, 32709, doi:10.1038/srep32709.

63. Battesti, A.; Majdalani, N.; Gottesman, S. Stress sigma factor RpoS degradation and translation are sensitive to the state of central metabolism. *Proceedings of the National Academy of Sciences* **2015**, *112*, 5159-5164, doi:10.1073/pnas.1504639112.

64. Rogers, A.; Townsley, L.; Gallego-Hernandez, A.L.; Beyhan, S.; Kwuan, L.; Yildiz, F.H. The LonA protease regulates biofilm formation, motility, virulence, and the Type VI secretion system in Vibrio cholerae. *J. Bacteriol.* **2016**, *198*, 973-985, doi:10.1128/jb.00741-15.

65. Marr, A.K.; Overhage, J.; Bains, M.; Hancock, R.E.W. The Lon protease of Pseudomonas aeruginosa is induced by aminoglycosides and is involved in biofilm formation and motility. *Microbiology (Read.)* **2007**, *153*, 474-482, doi:10.1099/mic.0.2006/002519-0.

66. Sugimoto, S.; Arita-Morioka, K.-i.; Terao, A.; Yamanaka, K.; Ogura, T.; Mizunoe, Y. Multitasking of Hsp70 chaperone in the biogenesis of bacterial functional amyloids. *Communications Biology* **2018**, *1*, 52, doi:10.1038/s42003-018-0056-0.

67. Prigent-Combaret, C.; Prensier, G.; Le Thi, T.T.; Vidal, O.; Lejeune, P.; Dorel, C. Developmental pathway for biofilm formation in curli-producing Escherichia coli strains : role of flagella, curli and colanic acid. *Environ. Microbiol.* **2000**, *2*, 450-464.

68. Abraham, J.N.; Nardin, C. Interaction of polymers with amyloidogenic peptides. *Polym. Int.* **2018**, *67*, 15-24, doi:10.1002/pi.5483.

69. Pratt, L.A.; Kolter, R. Genetic analysis of Escherichia coli biofilm formation : roles of flagella, motility, chemotaxis and type I pili. *Mol. Microbiol.* **1998**, *30*, 285-293.

70. Lillington, J.; Geibel, S.; Waksman, G. Biogenesis and adhesion of type 1 and P pili. *Biochim. Biophys. Acta* **2014**, *1840*, 2783-2793, doi:10.1016/j.bbagen.2014.04.021.

71. Thomas, W. Catch bonds in adhesion. *Annu. Rev. Biomed. Eng.* **2008**, *10*, 39-57, doi:10.1146/annurev.bioeng.10.061807.160427.

72. Persat, A.; Nadell, C.D.; Kim, M.K.; Ingremeau, F.; Siryaporn, A.; Drescher, K.; Wingreen, N.S.; Bassler, B.L.; Gitai, Z.; Stone, H.A. The mechanical world of bacteria. *Cell* **2015**, *161*, 988-997, doi:10.1016/j.cell.2015.05.005.

73. Kurylo, C.M.; Parks, M.M.; Juette, M.F.; Zinshteyn, B.; Altman, R.B.; Thibado, J.K.; Vincent, C.T.; Blanchard, S.C. Endogenous rRNA sequence variation can regulate stress response gene expression and phenotype. *Cell reports* **2018**, *25*, 236-248.e236, doi:10.1016/j.celrep.2018.08.093.

74. Uhlich, G.A.; Gunther, N.W.t.; Bayles, D.O.; Mosier, D.A. The CsgA and Lpp proteins of an Escherichia coli O157:H7 strain affect HEp-2 cell invasion, motility, and biofilm formation. *Infect. Immun.* **2009**, *77*, 1543-1552, doi:10.1128/iai.00949-08.

75. Sturgill, G.; Toutain, C.M.; Komperda, J.; O'Toole, G.A.; Rather, P.N. Role of CysE in production of an extracellular signaling molecule in Providencia stuartii and Escherichia coli: loss of CysE enhances biofilm formation in Escherichia coli. *J. Bacteriol.* **2004**, *186*, 7610-7617, doi:10.1128/jb.186.22.7610-7617.2004.

76. Rangel, D.E.; Marín-Medina, N.; Castro, J.E.; González-Mancera, A.; Forero-Shelton, M. Observation of bacterial Type I pili extension and contraction under fluid flow. *PLoS One* **2013**, *8*, e65563, doi:10.1371/journal.pone.0065563.

77. Hospenthal, M.K.; Zyla, D.; Costa, T.R.D.; Redzej, A.; Giese, C.; Lillington, J.; Glockshuber, R.; Waksman, G. The cryoelectron microscopy structure of the Type 1 chaperone-usher pilus rod. *Structure* **2017**, *25*, 1829-1838.e1824, doi:10.1016/j.str.2017.10.004.

78. Lauga, E.; DiLuzio, W.R.; Whitesides, G.M.; Stone, H.A. Swimming in circles: motion of bacteria near solid boundaries. *Biophys. J.* **2006**, *90*, 400-412, doi:10.1529/biophysj.105.069401.

79. Xu, H.; Dauparas, J.; Das, D.; Lauga, E.; Wu, Y. Self-organization of swimmers drives long-range fluid transport in bacterial colonies. *Nat. Commun.* **2019**, *10*, 1792, doi:10.1038/s41467-019-09818-2.

80. Song, F.; Brasch, M.E.; Wang, H.; Henderson, J.H.; Sauer, K.; Ren, D. How bacteria respond to material stiffness during attachment: a role of Escherichia coli flagellar motility. *ACS Appl. Mater. Interfaces* **2017**, *9*, 22176-22184, doi:10.1021/acsami.7b04757.

81. Hibbing, M.E.; Fuqua, C.; Parsek, M.R.; Peterson, S.B. Bacterial competition: surviving and thriving in the microbial jungle. *Nat. Rev. Microbiol.* **2010**, *8*, 15-25, doi:10.1038/nrmicro2259.

82. van der Westen, R.; Sjollema, J.; Molenaar, R.; Sharma, P.K.; van der Mei, H.C.; Busscher, H.J. Floating and tether-coupled adhesion of bacteria to hydrophobic and hydrophilic surfaces. *Langmuir* **2018**, *34*, 4937-4944, doi:10.1021/acs.langmuir.7b04331.

83. Sjollema, J.; van der Mei, H.C.; Hall, C.L.; Peterson, B.W.; de Vries, J.; Song, L.; Jong, E.D.d.; Busscher, H.J.; Swartjes, J.J.T.M. Detachment and successive re-attachment of multiple, reversibly-binding tethers result in irreversible bacterial adhesion to surfaces. *Scientific Reports* **2017**, *7*, 4369, doi:10.1038/s41598-017-04703-8.

84. Thomas, W.E.; Nilsson, L.M.; Forero, M.; Sokurenko, E.V.; Vogel, V. Shear-dependent 'stick-and-roll' adhesion of type 1 fimbriated Escherichia coli. *Mol. Microbiol.* **2004**, *53*, 1545-1557, doi:10.1111/j.1365-2958.2004.04226.x.

85. Holz, C.; Opitz, D.; Mehlich, J.; Ravoo, B.J.; Maier, B. Bacterial motility and clustering guided by microcontact printing. *Nano Lett.* **2009**, *9*, 4553-4557, doi:10.1021/nl903153c.

86. Zhang, R.; Ni, L.; Jin, Z.; Li, J.; Jin, F. Bacteria slingshot more on soft surfaces. *Nat. Commun.* **2014**, *5*, 5541, doi:10.1038/ncomms6541.

87. Maier, B.; Wong, G.C.L. How bacteria use Type IV pili machinery on surfaces. *Trends Microbiol.* **2015**, *23*, 775-788, doi:10.1016/j.tim.2015.09.002.

88. Sauvonnet, N.; Gounon, P.; Pugsley, A.P. PpdD Type IV pilin of Escherichia coli K-12 can be assembled into pili in Pseudomonas aeruginosa. *J. Bacteriol.* **2000**, *182*, 848-854, doi:10.1128/JB.182.3.848-854.2000.

89. Harshey, R.M. Bacterial motility on a surface: many ways to a common goal. *Annu. Rev. Microbiol.* **2003**, *57*, 249-273, doi:10.1146/annurev.micro.57.030502.091014.

90. Perez-Riverol, Y.; Bai, J.; Bandla, C.; García-Seisdedos, D.; Hewapathirana, S.; Kamatchinathan, S.; Kundu, D.J.; Prakash, A.; Frericks-Zipper, A.; Eisenacher, M.; et al. The PRIDE database resources in 2022: a hub for mass spectrometry-based proteomics evidences. *Nucleic Acids Res.* **2022**, *50*, D543-d552, doi:10.1093/nar/gkab1038.